Lyle, M., Koizumi, I., Richter, C., and Moore, T.C., Jr. (Eds.), 2000
Proceedings of the Ocean Drilling Program, Scientific Results, Vol. 167

11. MILLENNIAL-SCALE $CaCO_3$ AND C_{ORG} EVENTS ALONG THE NORTHERN AND CENTRAL CALIFORNIA MARGINS: STRATIGRAPHY AND ORIGINS[1]

Mitchell Lyle,[2] Alan Mix,[3] A. Christina Ravelo,[4] Dyke Andreasen,[4] Linda Heusser,[5] Annette Olivarez[2]

ABSTRACT

Sediments from five Leg 167 drill sites and three piston cores were analyzed for C_{org} and $CaCO_3$. Oxygen isotope stratigraphy on benthic foraminifers was used to assign age models to these sedimentary records. We find that the northern and central California margin is characterized by k.y.-scale events that can be found in both the $CaCO_3$ and C_{org} time series. We show that the $CaCO_3$ events are caused by changes in $CaCO_3$ production by plankton, not by dissolution. We also show that these $CaCO_3$ events occur in marine isotope Stages (MIS) 2, 3, and 4 during Dansgaard/Oeschger interstadials. They occur most strongly, however, on the MIS 5/4 glaciation and MIS 2/1 deglaciation. We believe that the link between the northeastern Pacific Ocean and North Atlantic is primarily transmitted by the atmosphere, not the ocean. Highest $CaCO_3$ production and burial occurs when the surface ocean is somewhat cooler than the modern ocean, and the surface mixed layer is somewhat more stable.

INTRODUCTION

Sediments in the northeastern Pacific Ocean are almost barren of $CaCO_3$ but relatively rich in C_{org}. Late Pleistocene marine sediments along the California margin, for example, average only about 3% $CaCO_3$ but ~1% C_{org}. Despite low average $CaCO_3$ contents, $CaCO_3$ time series have significant structure to them and show potential for paleoceanographic reconstructions (Karlin et al., 1992). Some events in the last 150 k.y. have five times the average $CaCO_3$ content and some sediments >400 ka reach 30% $CaCO_3$. In addition, it is known that numbers of short events can be found in marine isotope Stages (MIS) 3 and 4 (Karlin et al., 1992). These events should be useful to study oceanographic processes at the k.y. scale and to estimate sediment ages, provided that the events are chronostratigraphic. The stratigraphic objectives of this paper are (1) to test whether carbonate and organic carbon time series are chronostratigraphic, (2) to develop a detailed stratigraphy for the last 140 k.y., and (3) to develop a preliminary chronostratigraphy for the last 500 k.y. on the northern California margin. This will be accomplished using radiocarbon dating and oxygen isotope stratigraphy for absolute age control. Sufficient $CaCO_3$ is available above about 3500 m water depth to generate, with some difficulty, an oxygen isotope stratigraphy on benthic foraminifera to test whether these events are truly chronostratigraphic.

The high average sedimentation rates along the California margin have proved to be a mixed blessing for paleoceanographers. Although it is possible to generate records with submillennial resolution, the high sedimentation rates limit sampling to a short time interval. Until Leg 167, it was a rare core that unambiguously penetrated to MIS 5 and even rarer to MIS 6. Core EW9504-17PC from the Leg 167 site survey cruise, for example, reached 140 ka at 15 m below the sediment surface. Long time series of basic paleoceanographic measurements like $CaCO_3$ were simply not available prior to Leg 167. A further objective for this study is to generate a 500-k.y. record of carbon burial on the California margin to compare to other oceanographic regions.

Prior to Leg 167 it was known that k.y.-scale events occurred along the California margin (e.g., Santa Barbara Basin, Behl, and Kennett, 1996; Kennett, Baldauf, Lyle, et al., 1995), and that some of these events could be discerned in the $CaCO_3$ content and benthic stable isotope time series on the northern California margin (Karlin et al., 1992; Gardner et al., 1997; Lund and Mix, 1998). The final objective of this paper is to define the carbon time series sufficiently to compare to other regions, in particular the North Atlantic, and to determine to a first order the cause of the k.y.-scale $CaCO_3$ and C_{org} events.

Our strategy is to develop detailed age models for 0–140 ka for the $CaCO_3$ and C_{org} depth series at the eight sites we studied in detail (Table 1; Fig. 1), and to develop less precise age models for about the last 500 k.y. We used the sedimentation rates derived from these models combined with dry bulk density and carbon content to produce mass accumulation rate (MAR) models for the 0–140 ka period. For the northern/central California region we stacked these data to make robust estimates of percentage and MAR time series in the region. These data are used to compare to time series from the North Atlantic. We then briefly examine whether the events represent primarily changes in preservation or production of $CaCO_3$ and C_{org} along the California margin.

Core and Drill Site Locations

Figure 1 shows the site locations of cores or drill sites used in this study. We chose the northern sites (Sites 1019, 1020, and 1021, and Cores EW9504-17 and W8709-13) to form a depth transect from less than 1000 m below sea level (mbsl) to greater than 4000 mbsl. The

Table 1. Locations and water depths for cores and drill sites analyzed in this study.

Core or site designation	Latitude (°N)	Longitude (°W)	Water depth (mbsl)	Depth interval (mbsf)	Approximate time interval (ka)
EW9504-17PC	42°14.55′	125°49.82′	2671	0-15.09	0-140
W8709-13PC	42°07.01′	125°45.00′	2712	0-8.72	0-73
ODP Site 1019	41°40.97′	124°55.98′	988	0-65.73	0-255?
ODP Site 1020	41°00.05′	126°26.07′	3038	0-52.79	2-574
ODP Site 1021	39°05.25′	127°46.98′	4212	0-19.60	0-575
ODP Site 1018	36°59.39′	123°16.54′	2476	0-54.18	10-260
ODP Site 1011	31°16.82′	117°38.01′	2022	0-14.17	0-340
Y74-2-22P	23°43.80′	112°26.28′	3054	0-11.40	0-660

[1]Lyle, M., Koizumi, I., Richter, C., and Moore, T.C., Jr. (Eds.), 2000. *Proc. ODP, Sci. Results,* 167: College Station TX (Ocean Drilling Program).

[2]Center for Geophysical Investigation of the Shallow Subsurface, Boise State University, Boise ID 83725, USA. Correspondence author: mlyle@cgiss.boisestate.edu

[3]College of Ocean and Atmospheric Science, Oregon State University, Corvallis OR 97331, USA.

[4]Institute of Marine Sciences, University of California, Santa Cruz, Santa Cruz CA 95064, USA.

[5]Lamont-Doherty Geological Observatory, Columbia University, Palisades NY 10987, USA. (Present address: Heusser and Heusser, Inc., 100 Clinton Road, Tuxedo NY 10987, USA.)

other sites (Sites 1018 and 1011, and Core Y74-2-22) were chosen to form a transect along the California margin from ~40°N to the Tropic of Cancer.

ANALYTICAL METHODS

Oxygen Isotopes

Analytical methods are reported in detail in Mix et al. (1999) and Andreasen et al. (Chap. 8, this volume). Isotope data in this paper are from benthic foraminifers, primarily *Cibicidoides wuellerstorfii* and *Uvigerina* species.

Calcium Carbonate

All carbon analyses except the $CaCO_3$ analyses from Core W8709-13 were run at Boise State University. $CaCO_3$ analyses on core W8709-13 were run at Oregon State University using a UIC coulometer with an acidification module.

At Boise State University calcium carbonate was determined by coulometry using a UIC Inc. Model CM-5012 CO_2 coulometer attached to a modified version of the CM-5120 combustion furnace, schematically shown in Figure 2. Approximately 30–70 mg of dried, homogenized sediment sample was combusted in an ultra-high-purity oxygen (>99.994% O_2) atmosphere at 1000°C. The reported $CaCO_3$ data were calculated from two independent analyses of each sampled interval: first we measured the total carbon concentration and then the C_{org} fraction was measured in the second analysis after pretreatment with a 10% hydrochloric acid solution to dissolve solid $CaCO_3$. The carbonate carbon was calculated as the difference between the total carbon and the organic carbon fractions, and the $CaCO_3$ weight percent was calculated by multiplying carbonate carbon by 8.33.

We modified the CM-5120 furnace for marine sediment analysis because the residual sea salt caused premature breakage of the combustion tube. The CM-5120 furnace was designed with post-combustion scrubbers to remove impurities from the CO_2 gas evolved from sample combustion. Chlorine is removed as silver chloride by reaction with pure silver wire positioned at the end of the combustion tube. Residual sea salt produced excessive AgCl and formed a solid block in the combustion tube, resulting in breakage. We solved this problem by removing the silver from the UIC combustion tube and attaching a second tube furnace to the CM-5120 with teflon tubing for the chlorine scrubber. High-purity fused quartz tubing (7 mm outer diameter × 5 mm inner diameter × 610 mm length) was filled with ~15 g of pure silver wire and heated during the analysis to 475°C. The optimum operating temperature was determined to best remove chlorine from the gas stream after several trial and error experiments. This is based on the absence of a gas cloud in the cathode compartment of the titration cell, a stable cell current of zero mA (0 ± 1 mA) after sample analysis, and reproducible carbon measurements of in-house standards of several marine sediments also containing residual sea salt (Table 2).

We used the following acidification method to measure C_{org}. Approximately 70 mg of dried sample was placed inside a precleaned, custom made, high-purity fused quartz combustion boat (55 mm × 10 mm × 5 mm). The sample was wetted with four drops of water, and then with 10 drops of 10% HCl. The slurry was stirred with a glass stir rod and rinsed with four more drops of HCl, to wash back into the sample boat any sample adhering to the glass rod. This step prevented cross contamination between the sample boats and greatly improved the reproducibility of results. The fused quartz boats were heated at 110°C until sufficient solution evaporated to accommodate a second treatment with 10 drops of 10% HCl. Samples were oven dried and allowed to cool before analysis. We emphasize the importance of using fused quartz combustion boats. Previously, we had used a glazed porcelain boat (Coors Model #60032) but discovered the glaze deteriorated after about a dozen sample runs. Partial absorption of the sample slurry into the exposed porcelain produced erratic results and unacceptably high background readings.

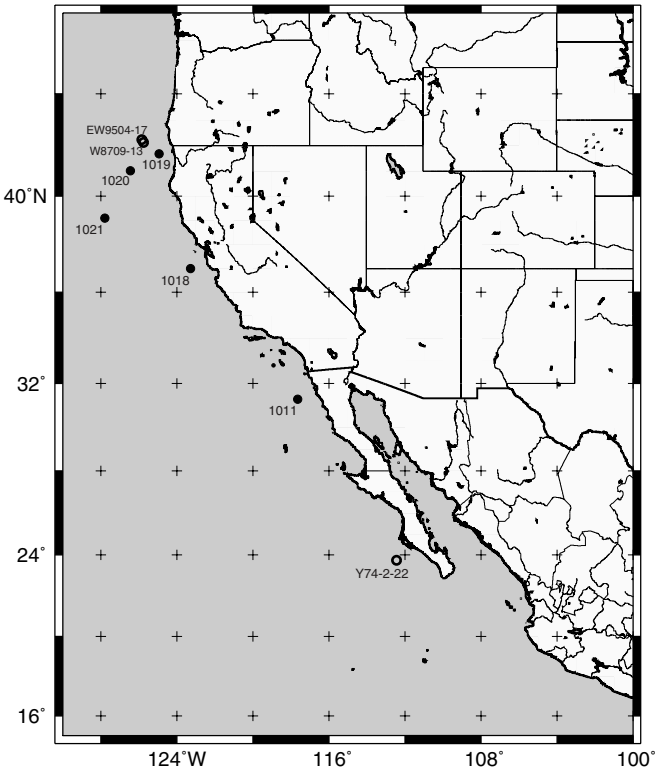

Figure 1. Map of California margin showing cores and drill sites used in this study. Open circles = piston cores, solid circles = ODP drill sites from Leg 167.

Precision and Accuracy

The accuracy and precision of the data were estimated by including two standards in each sample run and by repeat analyses of the unknown samples. For the standards we used a reagent-grade calcium carbonate and an in-house standard (SX27547, Gulf of California marine sediment) of a similar matrix as Leg 167 sediments. Two samples of the calcium carbonate reagent were analyzed at the beginning

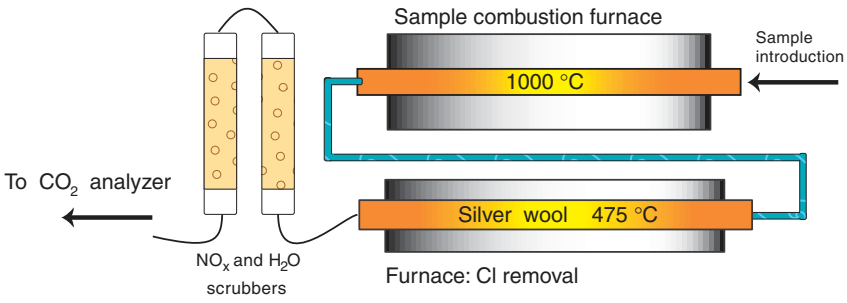

Figure 2. Schematic of carbon analysis showing Cl-removal furnace modification to run samples with high salt content (e.g., marine sediments).

and at the end each sample run. Four samples of the in-house standard were analyzed in a typical sample run: two samples of SX27547 were analyzed for total carbon and two for organic carbon following the acid treatment described above. Summary statistics for these standards are found in Table 2.

Precision was estimated by repeating the analysis of every fourth "unknown" sample in the sample run. The repeated analyses pertain to both the total carbon and organic carbon measurements. The average difference between the repeated samples is <0.01% carbon as shown in Table 3.

RESULTS

Carbon analyses were run at 5-cm intervals through 0–140 ka when possible (Figs. 3, 4) and at wider intervals below. Because of the different sedimentation rates (Fig. 5), sample spacing in years is somewhat variable. Sample spacing is about 500 yr in Site 1018 and Cores EW9504-17 and W8709-13, and at Site 1020 to about 28 revised meters composite depth (rmcd; ~ 250 ka; Table 4). Below that depth the sample spacing is ~2 k.y. For the other cores samples were spaced at ~3 k.y. in Core Y74-2-22, ~2 k.y. at Site 1011, ~1.5 k.y. at Site 1021, and varied from <0.1 to 3 k.y. at Site 1019. The data are reported in Tables 4–11.

It is clear from Figures 3 and 4 that there are $CaCO_3$ and C_{org} events common to the records along the California margin, and, as one would expect, sites close together are more similar than those more separated. We will discuss the trends and implications more below. First, however, we will discuss the development of the continuous sediment splice at each site and the development of the chronostratigraphy.

DEVELOPMENT OF STRATIGRAPHY

Strategy

Stratigraphy was developed by piecing together a continuous splice from the holes at each site, using the $CaCO_3$ and C_{org} time series to correlate between sites, and using benthic oxygen isotope time series to confirm that the correlations are indeed chronostratigraphic. We followed this method because we were beginning from reconnaissance-scale oxygen isotope records and because both the $CaCO_3$ and C_{org} time series have more bandwidth and thus a potential for a more constrained correlation. Any systematic problems between the "carbon" stratigraphy and the oxygen isotope stratigraphy would indicate a problem with the assumption that the $CaCO_3$ and C_{org} time series are chronostratigraphic.

We have established an age model for the 0- to 40-ka time period where we have adequate to excellent radiocarbon and oxygen isotope control. From 140 to 574 ka we have constructed a preliminary age model and warn readers that this age model will probably be revised as more data become available. We used the 0- to 140-ka ages to calculate MARs for this time period, as explained later.

For the Leg 167 drill sites we began by developing a continuous sediment column based initially on the shipboard splice (Lyle, Koizumi, Richter, et al., 1997). We revised the shipboard splice using our carbon records. For the most part the adjustments to the shipboard splice were minor, with the exception of the lower parts of Site 1019, as discussed in more detail below. Note that our revised offsets listed in Tables 4–11 are intended to be added to the meters below seafloor (mbsf) depth scale, not to the shipboard meters composite depth (mcd) scale, to obtain the revised scale (rmcd).

We then chose a few significant tie points between drill sites, based upon important oxygen isotope events (e.g., MIS 6/5 boundary) and any radiocarbon data we had, to begin correlation of the $CaCO_3$ and C_{org} time series. We used the program Analyseries 1.1 (Paillard et al., 1996) to correlate all records to a master site, Site 1020, in the depth domain. We alternately used each of the two carbon records to develop the correlation because they have significantly different time series (Figs. 3, 4). The final correlations shown in Tables 4–11 maximize the coherence from both records with Site 1020. By using both $CaCO_3$ and C_{org} records it was possible to spot correlations even if the amplitudes of the events in different cores were significantly different. We then used the depth correlation to Site 1020 to transfer an age scale from Site 1020 to the other cores. Finally we compared isotope records to confirm that the $CaCO_3$ and C_{org} time series are chronostratigraphic, and in some cases repeated the process when the carbon time series and isotopes disagreed.

Table 2. Carbon measurements—summary statistics for standards.

	$CaCO_3$ reagent	SX 27547
Average %C-total:	11.93	7.64
Standard deviation:	0.07	0.04
N:	773	77
Average %C-org:	NA	6.22
Standard deviation:		0.05
N:		69

Notes: %C-total = percent total carbon, %C-org = percent organic carbon.

Piston Cores W8709-13 and EW9504-17

We constructed the age model for 0–140 ka by correlations of the two piston Cores W8709-13 and EW9504-17 to Site 1020. Core W8709-13 was taken as part of the Multitracers transect (Table 1; Fig. 1; Lyle et al., 1992) and has a detailed chronostratigraphy in calendar ka to 57 ka (Lund and Mix, 1998). This chronostratigraphy is based upon 22 AMS radiocarbon dates on both planktic and benthic foraminifers to 35 ka and then upon correlation of millennial-scale oxygen isotope peaks to the north Atlantic Core V23-81 for the interval 36–57 ka. A recent radiocarbon compilation with some new dates

Table 3. Summary statistics and replicate precision.

Cruise:	Leg 167									Y-74-2	EW9504
Hole:	1021B	1021C	1020C	1020D	1019C	1019E	1018C	1018D	1011C	22 PC	17 PC
Average %C-total:	0.89	1.23	1.42	1.35	1.64	1.52	1.57	1.33	2.65	2.24	1.62
Standard deviation:	0.48	1.00	0.51	0.40	0.48	0.44	0.42	0.28	0.78	0.61	0.33
N:	134	237	521	225	440	311	494	62	145	229	300
Average %C-org:	0.56	0.50	0.89	0.88	1.20	1.04	1.30	1.06	1.41	1.35	1.23
Standard deviation:	0.12	0.07	0.20	0.18	0.36	0.25	0.34	0.25	0.34	0.32	0.30
N:	132	238	521	225	440	311	494	62	145	229	300
Average diff. %C-total:	0.007	0.007	0.009	0.008	0.012	0.011	0.009	0.010	0.018	0.020	0.015
Standard deviation:	0.007	0.007	0.008	0.007	0.017	0.009	0.008	0.007	0.016	0.017	0.013
N (replicates):	66	48	145	63	111	96	170	44	52	58	101
Average diff. %C-org:	0.006	0.004	0.005	0.007	0.010	0.005	0.009	0.012	0.017	0.016	0.012
Standard deviation:	0.006	0.003	0.006	0.008	0.014	0.004	0.009	0.012	0.018	0.013	0.011
N (replicates):	66	47	144	62	128	94	174	47	45	94	108

Notes: %C-total = percent total carbon, %C-org = percent organic carbon.

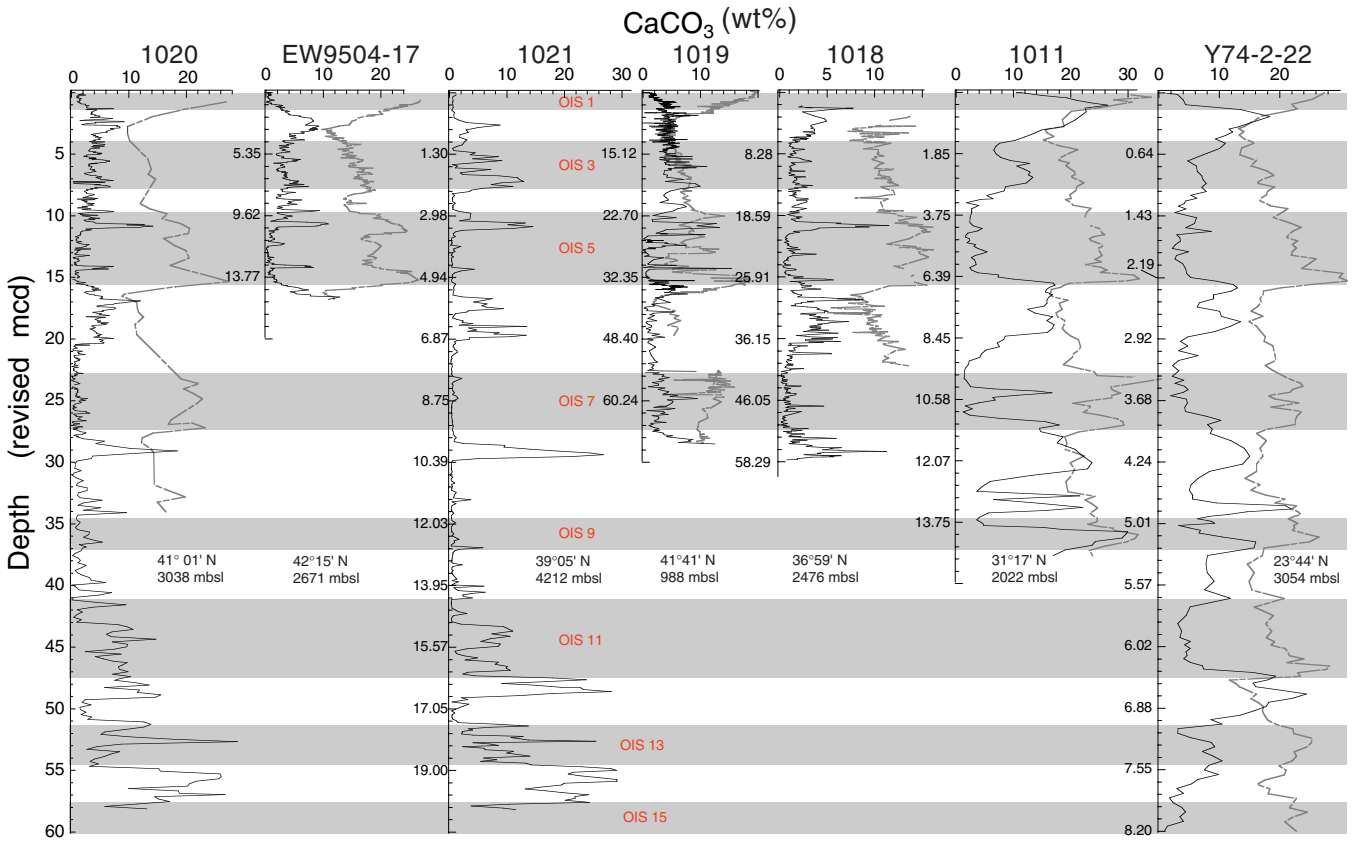

Figure 3. Weight percent $CaCO_3$ profiles in this study shown vs. depth and with benthic oxygen isotope time series superimposed where available. All profiles were originally plotted in Site 1020 equivalent depth derived from the correlations (see text) and then labeled with the local rmcd depth scale.

has also revised the Core W8709-13 age model somewhat (Mix et al., 1999). In this paper, we have chosen not to revise the 0–20 ka part of the time scale because the changes are relatively small. Instead we refer the readers to Mix et al. (1999) if they need the latest age model for this interval. $CaCO_3$ data used to correlate Cores W8709-13 and EW9504-17 are given in Table 5.

To continue the age model to 140 ka, we correlated Core W8709-13 to Core EW9504-17 taken about 15 km to the northwest on the site-survey cruise for Leg 167 (Table 1; Fig. 1). This 15-m piston core reached through MIS 5 to the end of MIS 6. It was measured at 5-cm intervals for $CaCO_3$ and C_{org} (Table 6). Benthic oxygen isotope time series of similar detail were also developed prior to the late Holocene by A.C. Mix (unpubl. data, Table 6). The three time series were used to correlate the two cores in detail and to transfer the age scale to Core EW9504-17. Below 57 ka, we used the isotope stratigraphy to develop an age model to 140 ka. We used the MIS time scale of Martinson et al. (1987) for this age model. For ages greater than 140 ka, we used the time scale of Martinson et al. (1987) to 300 ka, and used the Imbrie et al. (1984) time scale for older sediments.

Site 1020

We chose Site 1020 as our "master" site for the correlation, because we had sampled a record that spans >500 k.y. and sedimentation rates are sufficiently high to record high-frequency events, averaging 10 cm/k.y. for the entire Pleistocene. Unfortunately, Site 1020 has a few small turbidites most noticeably on the MIS 2/1 deglaciation (Table 4), which makes this a poor site to study the last ~15 k.y. in detail. To obtain the age model for 0–140 ka for Site 1020 we carefully correlated the carbon records with Core EW9504-17 and used reconnaissance-scale isotope measurements reported by A.C. Mix (unpubl. data) to confirm that the age model was reasonable. Again, we used the strategy to iterate between C_{org} and $CaCO_3$ correlation to maximize coherence in both time series and better constrain our stratigraphic model. Once we had an initial age model, we calculated sedimentation rates and reiterated the model to minimize sedimentation rate changes while still maintaining the high coherence between records (Fig. 6).

For sediments older than 140 ka (16.69 rmcd), we have a more difficult problem assigning age, and so we consider the age model from 148 to 574 ka preliminary. We have some oxygen isotope control to MIS 7 (Fig. 3) but little more is available now. Our other age control is based upon the last occurrence of the nannofossil *Pseudoemiliania lacunosa* (460 ka) at about 51 rmcd, the Brunhes/Matuyama paleomagnetic boundary at 84.83 mcd (780 ka; Lyle, Koizumi, Richter, et al., 1997), and pollen stratigraphy (Heusser et al., Chap. 17, this volume). One of the notable features of deglaciations at the MIS 5/6 and MIS 2/1 boundaries is an initial spike in alder (*Alnus*) pollen followed by oak (*Quercus*) and redwood (*Sequoia*). If we assume that this pattern is typical of deglaciations, we can date previous deglaciations below our oxygen isotope control (Fig. 7). The age model thus developed is in harmony with an age model developed by Kreitz et al. (Chap. 10, this volume) using alkenone SST estimates and assuming that cold SST marks glacials.

Site 1021

We had no isotope control for Site 1021 but established an initial age model from the *P. lacunosa* last occurrence datum (15.41–18.41 mcd; Fornaciari, Chap. 1, this volume) and the Brunhes/Matuyama paleomagnetic boundary (27.16 mcd; Lyle, Koizumi, Richter, et al., 1997). The final age model in Table 7 was refined by correlating the

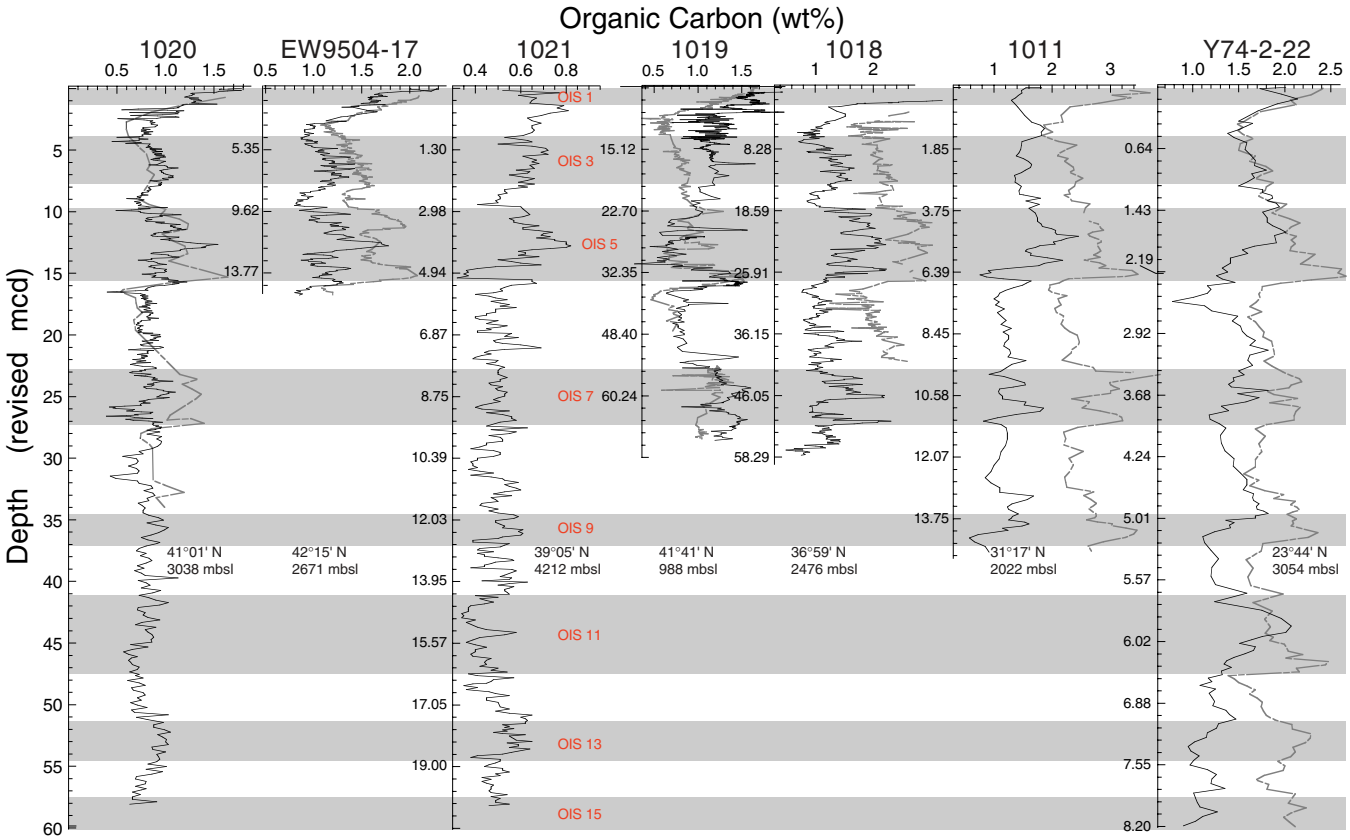

Figure 4. Weight percent C_{org} profiles in this study shown vs. depth and with benthic oxygen isotope time series superimposed where available. All profiles were originally plotted in Site 1020 equivalent depth derived from the correlations (see text) and then labeled with the local rmcd depth scale.

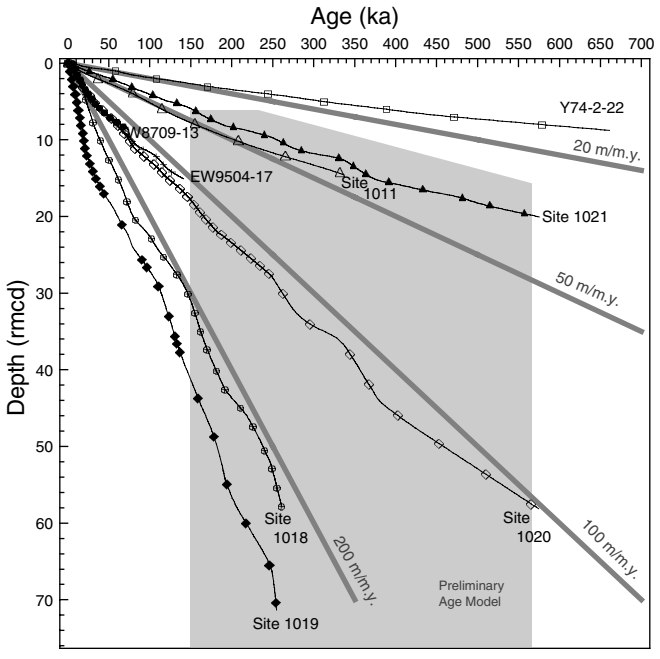

Figure 5. Depth/age plots of cores and drill sites in this study to show the levels of age resolution obtainable. The shaded region marks the depth intervals for Leg 167 drill sites with only a preliminary age model.

Site 1021 carbon records to Site 1020. After we completed our age model, we learned that Guyodo et al. (1999) had independently estimated ages using paleomagnetic intensity. Our age models agree well (±5 k.y.), except for the interval 360–480 ka, where we have an offset of about 40 k.y. between the two independent age models.

Site 1018

Site 1018 was relatively straightforward to correlate to Site 1020 (Table 8), and the benthic oxygen isotope time series (Andreasen et al., Chap. 8, this volume) is in agreement with the age model in Table 8. The main difficulties arose because Site 1018 is missing much of the Holocene, which is confirmed by the lack of a Holocene *Sequoia* pollen peak (L.E. Heusser, unpubl. data). A Holocene section was found in the site survey core (Core EW9504-13), so the missing section at Site 1018 is probably a recovery problem of the soft uppermost sediments, not a hiatus. The $CaCO_3$ and C_{org} correlations also presented a challenge. The peaks in Site 1018 were often significantly different in amplitude than Site 1020, and more iterations between the C_{org} and $CaCO_3$ time series were needed to achieve an optimum correlation. The differences in amplitude reflect some regionality in sedimentation, because this drill site is more than 500 km SSE of Site 1020.

Site 1019

Site 1019 is our problem child, with the promise of extremely high-resolution sections at the MIS 2/1 deglaciation (e.g., Mix et al., 1999) and at the MIS 5/6 boundary but with the difficulty of highly variable sedimentation. In addition, isotope measurements were not as clean to interpret as at other drill sites; we had problems with mis-

Table 4. Site 1020 splice carbon data.

Leg	Site	Hole	Core	Section	Interval Top (cm)	Interval Bottom (cm)	Average depth (mbsf)	Shipboard depth Offset (m)	Shipboard depth MCD (m)	Revised depth Offset (m)[1]	Revised depth RMCD (m)[2]	Age model (ka)[3]	Preliminary age model (>148 ka)	Sedimentation rate (cm/k.y.)	C_{org} (wt%)	$CaCO_3$ (wt%)	Wet bulk density (GRAPE; g/cm^3)	Estimated dry bulk density (g/cm^3)[4]	Bulk MAR (gm/cm^2/k.y.)[5]	C_{org} MAR (gm/cm^2/k.y.)[5]	$CaCO_3$ MAR (gm/cm^2/k.y.)[5]
167	1020	C	1H	1	2	3	0.03	0.00	0.03	0.00	0.06	1.99		15.46	1.58	2.33	1.50	0.77	11.96	0.189	0.28
167	1020	C	1H	1	5	6	0.06	0.00	0.06	0.00	0.11	2.17		15.46	1.56	2.03	1.50	0.77	11.96	0.186	0.24
167	1020	C	1H	1	10	11	0.11	0.00	0.11	0.00	0.17	2.48		15.13	1.56	1.36	1.50	0.77	11.71	0.182	0.16
167	1020	C	1H	1	15	18	0.17	0.00	0.17	0.00	0.21	2.87		14.75	1.82	2.51	1.50	0.77	11.41	0.207	0.29
167	1020	C	1H	1	20	21	0.21	0.00	0.21	0.00	0.26	3.14		14.35	1.64	1.19	1.50	0.77	11.10	0.182	0.13
167	1020	C	1H	1	25	26	0.26	0.00	0.26	0.00	0.31	3.49		14.02	1.55	1.08	1.50	0.77	10.84	0.168	0.12
167	1020	C	1H	1	30	31	0.31	0.00	0.31	0.00	0.36	3.84		13.72	1.52	1.52	1.50	0.77	10.61	0.162	0.16
167	1020	C	1H	1	35	38	0.37	0.00	0.37	0.00	0.43	4.28		13.49	1.28	1.10	1.50	0.77	10.43	0.133	0.11
167	1020	C	1H	1	40	41	0.41	0.00	0.41	0.00	0.46	4.58		13.28	1.26	1.38	1.50	0.77	10.27	0.130	0.14
167	1020	C	1H	1	45	46	0.46	0.00	0.46	0.00	0.51	4.96		13.14	1.30	1.94	1.50	0.77	10.16	0.132	0.20

Notes: [1] = revised, this paper, based upon correlation of carbon records in Holes 1020C and 1020D; see text for details. [2] = revised meters composite depth. [3] = ages from correlation to W8709-13 and EW9504; see text for details. [4] = dry bulk density estimated by linear correlation of Leg 167 index properties data: ρ dry = (1.563 ρ wet – 1.560). [5] = mass accumulation rate (MAR), or burial flux. Turbidite = turbidite interval in hole.

This is a sample of the table that appears on the volume CD-ROM.

Table 5. Age model, oxygen isotopes, and carbonate data for Core W8709-13.

Core	Average depth (cm)	Age (ka)*	$CaCO_3$ (%)†	C_{org} (wt%)‡
W8709-13PC	6	6.67	0.42	1.50
W8709-13PC	9	6.74	0.37	1.54
W8709-13PC	12	6.82	0.33	1.49
W8709-13PC	15	6.89	0.29	1.46
W8709-13PC	18	6.97	0.19	1.46
W8709-13PC	24	7.14	0.27	1.39
W8709-13PC	27	7.22	0.14	1.41
W8709-13PC	30	7.31	0.11	1.42
W8709-13PC	33	7.40	0.38	1.42
W8709-13PC	36	7.49	0.11	1.43
W8709-13PC	39	7.59	0.13	1.43
W8709-13PC	45	7.78	0.29	1.42
W8709-13PC	48	7.89	0.31	1.37
W8709-13PC	51	7.99	0.48	1.46
W8709-13PC	54	8.10	0.49	1.49
W8709-13PC	57	8.21	0.59	1.44
W8709-13PC	60	8.32	0.73	1.46
W8709-13PC	63	8.42	0.80	1.47
W8709-13PC	66	8.52	1.12	1.52
W8709-13PC	69	8.63	0.17	1.51
W8709-13PC	75	8.84	1.79	1.52
W8709-13PC	78	8.95	1.45	1.52
W8709-13PC	81	9.06	1.46	1.49
W8709-13PC	87	9.26	1.50	1.49
W8709-13PC	90	9.36	1.11	1.49
W8709-13PC	93	9.46	1.64	1.56
W8709-13PC	96	9.56	1.31	1.55
W8709-13PC	99	9.67	1.60	1.52
W8709-13PC	105	9.80	1.55	1.47
W8709-13PC	108	9.86	1.53	1.48
W8709-13PC	115	10.01	1.56	1.52
W8709-13PC	118	10.07	2.10	1.48
W8709-13PC	121	10.13	2.07	1.48
W8709-13PC	124	10.20	1.93	1.47
W8709-13PC	127	10.26	1.96	1.52
W8709-13PC	130	10.38	2.34	
W8709-13PC	133	10.51	1.93	1.60
W8709-13PC	136	10.65	1.99	1.45
W8709-13PC	139	10.78	1.97	1.47
W8709-13PC	145	10.91	1.54	1.36
W8709-13PC	148	11.03	1.58	1.30
W8709-13PC	154	11.26	2.22	1.24
W8709-13PC	157	11.34	2.47	1.20
W8709-13PC	160	11.42	2.15	1.29
W8709-13PC	163	11.50	2.39	1.28
W8709-13PC	166	11.57	3.59	
W8709-13PC	169	11.65	2.71	
W8709-13PC	172	11.73	2.78	1.38
W8709-13PC	178	11.89	2.80	1.39
W8709-13PC	181	11.97	2.98	1.35
W8709-13PC	184	12.05	3.16	1.33
W8709-13PC	187	12.32	3.46	1.35
W8709-13PC	190	12.98	4.37	1.47
W8709-13PC	193	13.64	3.96	1.48
W8709-13PC	196	14.30	3.53	1.42
W8709-13PC	199	14.70	4.82	1.29
W8709-13PC	202	14.84	4.43	1.28
W8709-13PC	205	14.97	4.64	1.25
W8709-13PC	208	15.11	4.46	1.19
W8709-13PC	211	15.25	5.45	1.17
W8709-13PC	214	15.38	6.09	1.21
W8709-13PC	217	15.52	6.38	1.27
W8709-13PC	220	15.65	7.11	1.19
W8709-13PC	223	15.77	6.15	1.10
W8709-13PC	225	15.84	5.97	1.06
W8709-13PC	228	15.93	5.13	0.99
W8709-13PC	231	16.01	1.98	0.89
W8709-13PC	234	16.09	6.89	1.12
W8709-13PC	237	16.18	6.43	1.15
W8709-13PC	240	16.27	6.38	1.12
W8709-13PC	243	16.35	6.29	1.11
W8709-13PC	246	16.43	6.54	1.07
W8709-13PC	249	16.52	6.90	0.97
W8709-13PC	252	16.60	6.03	0.87
W8709-13PC	258	16.77	7.60	0.92
W8709-13PC	262	16.88	6.43	0.90
W8709-13PC	265	16.97	6.40	0.90
W8709-13PC	268	17.05	7.22	0.90
W8709-13PC	274	17.28	7.11	0.87
W8709-13PC	277	17.47	7.02	0.88
W8709-13PC	280	17.66	5.80	0.88
W8709-13PC	283	17.85	5.97	0.92
W8709-13PC	286	18.04	7.01	0.90
W8709-13PC	289	18.24	7.22	0.90
W8709-13PC	292	18.43	7.02	0.92
W8709-13PC	295	18.62	6.67	
W8709-13PC	298	18.81	5.28	0.88
W8709-13PC	301	19.00	5.49	0.90
W8709-13PC	304	19.19	4.58	0.85
W8709-13PC	307	19.37	5.64	0.90
W8709-13PC	310	19.55	6.61	0.92
W8709-13PC	313	19.73	6.70	0.93
W8709-13PC	316	19.91	4.29	0.87
W8709-13PC	319	20.09	4.14	0.86
W8709-13PC	325	20.45	3.29	0.79
W8709-13PC	328	20.63	2.97	0.85
W8709-13PC	331	20.81	3.28	0.87
W8709-13PC	334	20.99	3.32	
W8709-13PC	337	21.17	3.16	0.88
W8709-13PC	340	21.34	2.99	0.85
W8709-13PC	343	21.52	3.50	
W8709-13PC	346	21.70	3.31	
W8709-13PC	349	21.87	4.08	
W8709-13PC	352	22.05	3.84	
W8709-13PC	355	22.23	3.27	
W8709-13PC	358	22.40	3.20	
W8709-13PC	361	22.58	3.54	
W8709-13PC	364	22.76	3.25	
W8709-13PC	367	22.93	3.16	
W8709-13PC	370	23.11	4.36	
W8709-13PC	373	23.29	4.25	
W8709-13PC	376	23.47	4.82	
W8709-13PC	379	23.64	3.53	
W8709-13PC	382	23.82	2.26	
W8709-13PC	385	24.00	2.98	
W8709-13PC	388	24.17	2.64	
W8709-13PC	391	24.35	2.17	
W8709-13PC	394	24.56	1.75	
W8709-13PC	397	24.79	1.90	
W8709-13PC	400	25.01	1.77	
W8709-13PC	403	25.24	1.94	
W8709-13PC	406	25.46	2.20	
W8709-13PC	409	25.69	2.77	
W8709-13PC	412	25.92	3.31	
W8709-13PC	415	26.14	3.16	
W8709-13PC	418	26.37	3.23	
W8709-13PC	421	26.59	3.11	
W8709-13PC	424	26.82	3.41	
W8709-13PC	427	27.04	3.79	
W8709-13PC	430	27.27	1.71	
W8709-13PC	433	27.50	2.62	
W8709-13PC	436	27.72	3.96	
W8709-13PC	439	27.95	2.65	
W8709-13PC	442	28.17	2.75	
W8709-13PC	445	28.38	3.15	
W8709-13PC	448	28.59	1.86	
W8709-13PC	451	28.79	2.13	
W8709-13PC	454	28.99	1.91	
W8709-13PC	457	29.20	1.64	
W8709-13PC	460	29.40	1.52	
W8709-13PC	463	29.60	1.16	
W8709-13PC	466	29.81	1.25	
W8709-13PC	469	30.01	1.31	
W8709-13PC	472	30.21	2.30	
W8709-13PC	475	30.42	1.44	
W8709-13PC	478	30.62	1.66	
W8709-13PC	481	30.82	2.14	
W8709-13PC	484	31.03	1.82	
W8709-13PC	487	31.23	1.97	
W8709-13PC	490	31.43	1.83	
W8709-13PC	493	31.64	1.95	
W8709-13PC	496	31.84	3.25	
W8709-13PC	499	32.04	3.64	
W8709-13PC	502	32.25	2.46	
W8709-13PC	505	32.45	2.02	
W8709-13PC	508	32.65	1.65	
W8709-13PC	511	32.84	1.48	
W8709-13PC	514	33.05	1.90	
W8709-13PC	517	33.25	2.39	
W8709-13PC	520	33.45	1.12	
W8709-13PC	523	33.65	1.39	
W8709-13PC	526	33.85	1.16	
W8709-13PC	529	34.05	1.42	
W8709-13PC	532	34.25	1.62	
W8709-13PC	535	34.45	2.10	
W8709-13PC	538	34.65	1.79	
W8709-13PC	541	34.85	1.75	
W8709-13PC	544	35.05	1.59	
W8709-13PC	547	35.25	2.74	
W8709-13PC	550	35.45	2.44	
W8709-13PC	553	35.65	3.66	
W8709-13PC	556	35.85	2.80	
W8709-13PC	559	36.15	2.88	
W8709-13PC	562	36.49	3.25	
W8709-13PC	566	36.95	3.22	
W8709-13PC	569	37.29	3.10	

Table 5 (continued).

Core	Average depth (cm)	Age (ka)*	$CaCO_3$ (%)†	C_{org} (wt%)‡
W8709-13PC	572	37.54	2.87	
W8709-13PC	575	37.74	2.46	
W8709-13PC	578	37.95	1.82	
W8709-13PC	581	38.15	1.87	
W8709-13PC	584	38.36	2.50	
W8709-13PC	587	38.56	2.22	
W8709-13PC	590	38.77	2.34	
W8709-13PC	593	38.97	2.38	
W8709-13PC	596	39.18	1.16	
W8709-13PC	599	39.38	2.04	
W8709-13PC	602	39.59	1.45	
W8709-13PC	605	39.79	1.60	
W8709-13PC	608	40.00	1.99	
W8709-13PC	611	40.39	1.72	
W8709-13PC	614	40.78	1.39	
W8709-13PC	617	41.17	2.06	
W8709-13PC	620	41.56	1.42	
W8709-13PC	623	41.95	2.11	
W8709-13PC	626	42.34	1.23	
W8709-13PC	629	42.73	1.69	
W8709-13PC	632	43.12	1.09	
W8709-13PC	635	43.51	1.17	
W8709-13PC	638	43.90	2.46	
W8709-13PC	641	44.29	1.81	
W8709-13PC	644	44.68	1.63	
W8709-13PC	647	45.07	2.72	
W8709-13PC	650	45.46	2.45	
W8709-13PC	653	45.85	2.64	
W8709-13PC	656	46.24	2.02	
W8709-13PC	659	46.61	1.60	
W8709-13PC	662	46.96	1.70	
W8709-13PC	665	47.31	1.63	
W8709-13PC	668	47.66	1.84	
W8709-13PC	671	48.01	1.89	
W8709-13PC	674	48.36	1.92	
W8709-13PC	677	48.71	1.87	
W8709-13PC	680	49.06	2.11	
W8709-13PC	683	49.41	2.26	
W8709-13PC	686	49.75	2.34	
W8709-13PC	689	50.10	2.02	
W8709-13PC	692	50.45	2.14	
W8709-13PC	695	50.80	2.22	
W8709-13PC	698	51.24	2.45	
W8709-13PC	701	51.68	2.86	
W8709-13PC	704	52.12	2.16	
W8709-13PC	707	52.56	2.12	
W8709-13PC	710	53.00	2.19	
W8709-13PC	713	53.48	3.34	
W8709-13PC	719	54.44	4.04	
W8709-13PC	722	54.92	3.24	
W8709-13PC	725	55.40	3.66	
W8709-13PC	728	55.88	2.82	
W8709-13PC	731	56.36	1.72	
W8709-13PC	734	56.84	2.57	
W8709-13PC	737	57.16	2.58	
W8709-13PC	740	57.40	3.00	
W8709-13PC	743	57.64	2.70	
W8709-13PC	746	57.88	2.48	
W8709-13PC	749	58.12	2.36	
W8709-13PC	752	58.36	1.19	
W8709-13PC	755	58.60	1.43	
W8709-13PC	758	58.84	2.10	
W8709-13PC	761	59.15	2.53	
W8709-13PC	764	59.60	2.48	
W8709-13PC	767	60.05	1.77	
W8709-13PC	770	60.51	1.98	
W8709-13PC	773	60.98	1.77	
W8709-13PC	776	61.46	1.51	
W8709-13PC	779	61.58	1.40	
W8709-13PC	782	61.71	1.01	
W8709-13PC	785	62.27	0.99	
W8709-13PC	788	62.85	1.33	
W8709-13PC	791	63.45	1.36	
W8709-13PC	794	64.07	1.64	
W8709-13PC	797	64.70	0.83	
W8709-13PC	800	65.20	3.32	
W8709-13PC	803	65.30	2.48	
W8709-13PC	806	65.59	1.61	
W8709-13PC	809	66.01	1.58	
W8709-13PC	812	66.47	0.96	
W8709-13PC	815	66.95	1.46	
W8709-13PC	818	67.15	1.33	
W8709-13PC	821	67.37	2.43	
W8709-13PC	824	67.63	2.02	
W8709-13PC	827	67.95	3.25	
W8709-13PC	830	68.38	2.62	
W8709-13PC	833	68.84	2.65	
W8709-13PC	836	69.29	0.81	
W8709-13PC	839	69.74	2.11	
W8709-13PC	842	70.19	1.42	
W8709-13PC	845	70.62	1.25	
W8709-13PC	848	71.05	1.05	
W8709-13PC	851	71.46	1.29	
W8709-13PC	854	71.86	6.12	
W8709-13PC	857	72.26	6.68	
W8709-13PC	860	72.67	4.69	
W8709-13PC	863	73.07	1.97	
W8709-13PC	866	73.49	2.89	
W8709-13PC	869	73.91	2.21	

Notes: * = age model and isotope data are from Lund and Mix (1998). Below 800 cm the age model has been adjusted based upon EW9504-17 correlations. † = Analyses run at Oregon State University. ‡ = Analyses run at Boise State University.

Table 6. Data from Core EW9504-17P, including the age model and benthic oxygen isotopes.

Core	Interval Top (cm)	Interval Bottom (cm)	Average depth (m)	Age model (ka)	Sedimentation rate (cm/k.y.)	O^{18} (uvi-scale) per mil[1]	Site 1020 equivalent depth (m)[2]	Average C_{org}	$CaCO_3$ (%)	Wet bulk density (GRAPE; gm/cm^3)	Dry bulk density (estimated[3]; gm/cm^3)	Bulk MAR[4] ($gm/cm^2/k.y.$)	C_{org} MAR[4] ($g/cm^2/k.y.$)	$CaCO_3$ MAR[4] ($g/cm^2/k.y.$)
EW9504-17PC	0	2	0.01	0.08	12.297		0.012	2.013	0.18	1.29	0.461	5.669	0.114	0.010
EW9504-17PC	5	7	0.06	0.49	12.297		0.073	2.000	0.82	1.31	0.492	6.050	0.121	0.050
EW9504-17PC	10	11	0.105	0.85	12.297		0.128	2.095	0.62	1.33	0.524	6.444	0.135	0.040
EW9504-17PC	15	17	0.16	1.30	12.297		0.195	2.145	0.92	1.33	0.524	6.444	0.138	0.059
EW9504-17PC	20	22	0.21	1.71	12.297		0.256	2.223	0.39	1.34	0.54	6.640	0.148	0.026
EW9504-17PC	25	27	0.26	2.11	12.297		0.044	2.287	0.48	1.35	0.556	6.837	0.156	0.033
EW9504-17PC	30	32	0.31	2.52	12.297		0.111	2.288	0.31	1.32	0.508	6.247	0.143	0.019
EW9504-17PC	40	42	0.41	3.33	12.297		0.233	2.111	0.74	1.34	0.54	6.640	0.140	0.049
EW9504-17PC	45	47	0.46	3.74	12.297		0.290	1.910	0.46	1.35	0.556	6.837	0.131	0.031
EW9504-17PC	50	52	0.51	4.15	12.297		0.347	1.770	0.25	1.36	0.572	7.034	0.124	0.018

Notes: [1] = A.C. Mix, unpublished data. [2] = equivalent revised meters composite depth interval in Site 1020 based on correlating the two time series. [3] = dry bulk density estimated by linear correlation of Leg 167 index properties data: ρ dry = (1.563 ρ wet – 1.560). [4] = mass accumulation rate (MAR), or burial flux.

This is a sample of the table that appears on the volume CD-ROM.

Table 7. Data from Site 1021 composite section.

Leg	Site	Hole	Core	Section	Interval Top (cm)	Interval Bottom (cm)	Average depth (mbsf)	Shipboard depth Offset (m)	Shipboard depth MCD (m)	Site 1020 equivalent depth (m)[1]	Age model (ka)[1]	Sedimentation rate (cm/k.y.)	C_{org} (wt%)	$CaCO_3$ (wt%)	Wet bulk density (GRAPE; g/cm^3)	Estimated dry bulk density (g/cm^3)[2]	Bulk MAR[3] (gm/cm^2/k.y.)	C_{org} MAR (gm/cm^2/k.y.)[3]	$CaCO_3$ MAR (gm/cm^2/k.y.)[3]
167	1021	B	1H	1	5	6	0.055	0.00	0.055	0.17	1.67	3.30	0.52	1.05	1.48	0.74	2.45	0.013	0.026
167	1021	B	1H	1	10	11	0.105	0.00	0.105	0.38	3.18	3.30	0.77	0.34	1.48	0.74	2.45	0.019	0.008
167	1021	B	1H	1	15	16	0.155	0.00	0.155	0.58	4.70	3.30	0.59	0.43	1.48	0.74	2.45	0.014	0.011
167	1021	B	1H	1	20	21	0.205	0.00	0.205	0.79	6.21	3.54	0.67	0.41	1.49	0.76	2.69	0.018	0.011
167	1021	B	1H	1	25	26	0.255	0.00	0.255	1.00	7.53	4.04	0.65	0.45	1.52	0.80	3.25	0.021	0.015
167	1021	B	1H	1	30	31	0.305	0.00	0.305	1.20	8.69	4.59	0.64	0.54	1.53	0.82	3.77	0.024	0.020
167	1021	B	1H	1	35	36	0.355	0.00	0.355	1.41	9.71	4.90	0.79	0.25	1.53	0.82	4.02	0.032	0.010
167	1021	B	1H	1	40	41	0.405	0.00	0.405	1.61	10.73	5.10	0.76	0.73	1.51	0.79	4.02	0.031	0.029
167	1021	B	1H	1	45	46	0.455	0.00	0.455	1.82	11.67	5.30	0.81	0.63	1.50	0.77	4.10	0.033	0.026
167	1021	B	1H	1	50	51	0.505	0.00	0.505	2.02	12.62	5.30	0.73	0.67	1.51	0.79	4.18	0.031	0.028

Notes: [1] = equivalent revised meters composite depth interval in Site 1020 and age model established by correlating Site 1021 with Site 1020. [2] = dry bulk density estimated by linear correlation of Leg 167 index properties data: ρ dry = (1.563 ρ wet – 1.560). [3] = mass accumulation rate (MAR), or burial flux.

This is a sample of the table that appears on the volume CD-ROM.

Table 8. Data from Site 1018 composite section, with revised MCD and using age model in which MIS 5/4 boundary is at 24.4 RMCD.

Leg	Site	Hole	Core	Section	Interval Top (cm)	Interval Bottom (cm)	Average depth (mbsf)	Shipboard depth Offset (m)	Shipboard depth MCD (m)	Revised depth Offset (m)	Revised depth RMCD (m)	Site 1020 equivalent depth (m)[1]	Age model (ka)	Sedimentation rate (cm/k.y.)	C_{org} (wt%)	$CaCO_3$ (wt%)	Wet bulk density (GRAPE; g/cm^3)	Estimated dry bulk density (g/cm^3)[2]	Bulk MAR (g/cm^2/k.y.)[3]	C_{org} MAR (g/cm^2/k.y.)[3]	$CaCO_3$ MAR (g/cm^2/k.y.)[3]
167	1018	C	1H	1	4	8	0.06	–0.08	–0.02	–0.08	–0.02	1.07			3.18	2.43	1.50	0.77			
167	1018	C	1H	1	15	18	0.17	–0.08	0.09	–0.08	0.09	1.10			3.01	2.34	1.50	0.77			
167	1018	C	1H	1	24	28	0.26	–0.08	0.18	–0.08	0.18	1.13			2.91	2.35	1.50	0.77			
167	1018	C	1H	1	46	50	0.48	–0.08	0.40	–0.08	0.40	1.18			2.51	2.20	1.50	0.77			
167	1018	C	1H	1	55	58	0.57	–0.08	0.49	–0.08	0.49	1.20			2.43	2.01	1.50	0.77			
167	1018	C	1H	1	64	68	0.66	–0.08	0.58	–0.08	0.58	1.22			2.43	2.84	1.50	0.77			
167	1018	C	1H	1	75	78	0.77	–0.08	0.69	–0.08	0.69	1.23			2.32	2.80	1.50	0.77			
167	1018	C	1H	1	84	88	0.86	–0.08	0.78	–0.08	0.78	1.25			2.26	3.44	1.51	0.79			
167	1018	C	1H	1	104	108	1.06	–0.08	0.98	–0.08	0.98	1.29			1.87	7.02	1.51	0.79			
167	1018	C	1H	1	115	118	1.17	–0.08	1.09	–0.08	1.09	1.31			1.84	7.72	1.52	0.80			

Notes: [1] = equivalent revised meters composite depth interval in Site 1020 and age model established by correlating Site 1018 with Site 1020. [2] = dry bulk density estimated by linear correlation of Leg 167 index properties data: ρ dry = (1.563 ρ wet – 1.560). [3] = mass accumulation rate (MAR), or burial flux.

This is a sample of the table that appears on the volume CD-ROM.

Table 9. Site 1019 splice carbon data.

Leg	Site	Hole	Core	Section	Interval Top (cm)	Interval Bottom (cm)	Average depth (mbsf)	Shipboard depth Offset (m)	Shipboard depth MCD (m)	Revised depth Offset (m)	Revised depth RMCD (m)	Site 1020 equivalent depth (m)[1]	Age model (ka)	Sedimentation rate (cm/k.y.)	C_{org} (wt%)	$CaCO_3$ (wt%)	Wet bulk density (GRAPE; g/cm^3)	Estimated dry bulk density (g/cm^3)[2]	Bulk MAR (g/cm^2/k.y.)[3]	C_{org} MAR (g/cm^2/k.y.)[3]	$CaCO_3$ MAR (g/cm^2/k.y.)[3]
167	1019	C	1H	1	5	7	0.06	0.00	0.06	0.00	0.06	0.03	0.14	0.43	2.13	1.37	1.50	0.77	33.52	0.714	0.46
167	1019	C	1H	1	10	12	0.11	0.00	0.11	0.00	0.11	0.04	0.25	0.43	2.08	1.37	1.50	0.77	33.52	0.697	0.46
167	1019	C	1H	1	15	19	0.17	0.00	0.17	0.00	0.17	0.05	0.39	0.43	2.15	1.54	1.50	0.77	33.52	0.721	0.52
167	1019	C	1H	1	20	22	0.21	0.00	0.21	0.00	0.21	0.06	0.48	0.43	2.16	1.37	1.50	0.77	33.52	0.724	0.46
167	1019	C	1H	1	25	27	0.26	0.00	0.26	0.00	0.26	0.07	0.60	0.43	2.17	1.07	1.50	0.77	33.52	0.727	0.36
167	1019	C	1H	1	30	32	0.31	0.00	0.31	0.00	0.31	0.08	0.72	0.43	2.14	1.23	1.53	0.82	35.52	0.760	0.44
167	1019	C	1H	1	35	37	0.36	0.00	0.36	0.00	0.36	0.09	0.83	0.43	2.06	1.38	1.54	0.84	36.19	0.746	0.50
167	1019	C	1H	1	40	45	0.43	0.00	0.43	0.00	0.43	0.10	0.99	0.43	2.03	2.13	1.54	0.84	36.19	0.735	0.77
167	1019	C	1H	1	45	47	0.46	0.00	0.46	0.00	0.46	0.11	1.06	0.43	2.00	1.16	1.54	0.84	36.19	0.724	0.42
167	1019	C	1H	1	50	52	0.51	0.00	0.51	0.00	0.51	0.12	1.18	0.43	2.00	1.28	1.55	0.85	36.86	0.737	0.47

Notes: [1] = equivalent revised meters composite depth interval in Site 1020 and age model established by correlating Site 1019 with Site 1020 and by radiocarbon control in the 0–20 ka interval. [2] = dry bulk density estimated by linear correlation of Leg 167 index properties data: ρ dry = (1.563 ρ wet – 1.560). [3] = mass accumulation rate (MAR), or burial flux.

This is a sample of the table that appears on the volume CD-ROM.

Table 10. Data from Site 1011 composite section, with revised MCD and age model.

Leg	Site	Hole	Core	Section	Interval Top (cm)	Interval Bottom (cm)	Average depth (mbsf)	Shipboard depth Offset (m)	Shipboard depth MCD (m)	Site 1020 equivalent depth (m)[1]	Age model (ka)	Sedimentation rate (cm/k.y.)	C_{org} (wt%)	$CaCO_3$ (wt%)	Wet bulk density (GRAPE; g/cm^3)	Estimated dry bulk density (g/cm^3)[2]	Bulk MAR (g/cm^2/k.y.)[3]	C_{org} MAR (g/cm^2/k.y.)[3]	$CaCO_3$ MAR (g/cm^2/k.y.)[3]
167	1011	C	1H	1	2	5	0.04	0.00	0.04	0.03	0.21	7.02	1.82	10.45	1.45	0.70	4.89	0.089	0.511
167	1011	C	1H	1	15	18	0.17	0.00	0.17	0.04	2.06	7.02	1.55	11.43	1.47	0.73	5.11	0.079	0.584
167	1011	C	1H	1	25	28	0.27	0.00	0.27	0.25	3.48	6.96	1.47	14.92	1.48	0.74	5.17	0.076	0.771
167	1011	C	1H	1	35	38	0.37	0.00	0.37	0.45	4.93	6.87	1.48	19.31	1.50	0.77	5.31	0.079	1.026
167	1011	C	1H	1	45	48	0.47	0.00	0.47	0.64	6.40	6.75	1.42	21.03	1.52	0.80	5.43	0.077	1.142
167	1011	C	1H	1	55	58	0.57	0.00	0.57	0.84	7.89	6.55	1.37	23.35	1.51	0.79	5.17	0.071	1.207
167	1011	C	1H	1	65	68	0.67	0.00	0.67	1.05	9.42	6.55	1.30	26.45	1.52	0.80	5.27	0.068	1.393
167	1011	C	1H	1	75	78	0.77	0.00	0.77	1.30	11.00	6.32	1.35	22.48	1.54	0.84	5.28	0.071	1.186
167	1011	C	1H	1	85	88	0.87	0.00	0.87	1.59	12.62	6.06	1.41	22.73	1.55	0.85	5.15	0.073	1.172
167	1011	C	1H	1	95	98	0.97	0.00	0.97	2.27	14.30	5.85	1.53	20.71	1.54	0.84	4.89	0.075	1.012

Notes: [1] = equivalent revised meters composite depth interval in Site 1020 and age model established by correlating Site 1018 with Site 1020. [2] = Dry bulk density estimated by linear correlation of Leg 167 index properties data: ρ dry = (1.563 ρ wet – 1.560). [3] = mass accumulation rate (MAR), or burial flux.

This is a sample of the table that appears on the volume CD-ROM.

Table 11. Data from Core Y74-2-22PC, with benthic oxygen isotopes and age model.

Core	Average depth (m)	Age model (ka)	Sedimentation rate (cm/k.y.)	Site 1020 equivalent depth (m)[1]	O^{18} (uvi-scale) per mil[2]	C_{org} (wt%)	$CaCO_3$ (wt%)	Estimated dry bulk density (g/cm^3)[3]	Bulk MAR[4] (g/cm^2/k.y.)	C_{org} MAR[4] (g/cm^2/k.y.)	$CaCO_3$ MAR[4] (g/cm^2/k.y.)
Y74-2-22	0.01	0.21	1.54	0.03	3.50	2.01	1.29	0.79	1.218	0.024	0.016
Y74-2-22	0.05	2.68	1.54	0.14	3.53	1.73	3.04	0.79	1.220	0.021	0.037
Y74-2-22	0.10	5.88	1.62	0.58	3.71	1.96	3.99	0.79	1.286	0.025	0.051
Y74-2-22	0.15	8.85	1.80	0.97	4.07	2.14	4.41	0.79	1.428	0.031	0.063
Y74-2-22	0.20	11.44	2.11	1.38	3.96	1.92	13.50	0.80	1.680	0.032	0.227
Y74-2-22	0.25	13.58	2.56	1.92	4.58	1.71	18.34	0.80	2.045	0.035	0.375
Y74-2-22	0.31	15.73	2.89	2.77	4.88	1.50	13.12	0.80	2.312	0.035	0.303
Y74-2-22	0.35	17.04	3.03	2.96	4.98	1.65	11.59	0.80	2.429	0.040	0.282
Y74-2-22	0.40	18.70	2.86	3.19	4.89	1.58	12.21	0.80	2.299	0.036	0.281
Y74-2-22	0.45	20.53	2.49	3.46	4.97	1.50	11.05	0.80	2.001	0.030	0.221

Notes: [1] = equivalent revised meters composite depth interval in Site 1020 based on correlating the two time series. [2] = A.C. Mix, unpubl. data. [3] = Dry bulk density estimated by 2nd order fit of dry bulk density to depth in Site 1011. [4] = Mass accumulation rate (MAR) or burial flux.

This is a sample of the table that appears on the volume CD-ROM.

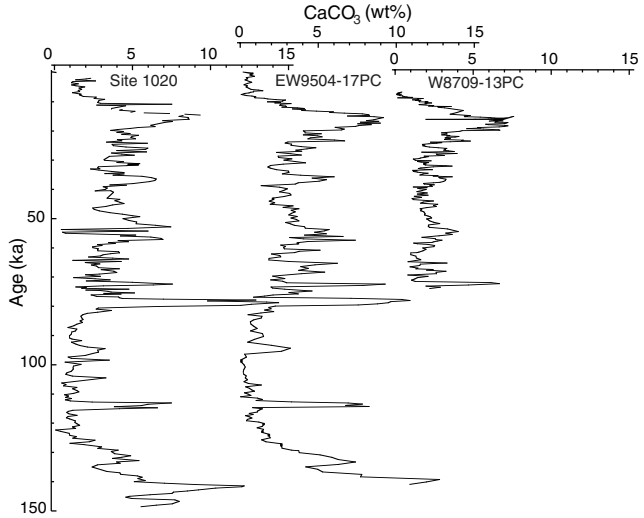

Figure 6. Weight percent $CaCO_3$ records for the period 0–140 ka used to transfer an age model from piston Cores W8709-13 (Lund and Mix, 1998) and EW9504-17 to Site 1020.

labeled samples, and we sampled at a coarser resolution (30-cm spacing) than the other drill sites. Despite these difficulties, we have developed an age model for about 0–250 ka, with an average sedimentation rate near 30 cm/k.y.

We are in the process of rerunning the carbon analyses on this core at a sample spacing of 5 cm. We report data at this spacing from 0 to 17.5 rmcd, or for the time interval 0–44 ka. The more detailed sampling has improved our confidence in correlations to other Leg 167 drill sites.

Site 1019 is the only site we studied that has major differences between the shipboard composite section and the revised section (Table 9). We redid the composite section on Holes 1019C and 1019E using magnetic susceptibility, color reflectance, $CaCO_3$, and C_{org}. We did not use the gamma-ray attenuation porosity evaluator (GRAPE) bulk density data, because the site was very gassy and we were concerned that the GRAPE data had many coring artifacts. The additional time series resolved several ambiguities in creating the composite section. For example, a dolomitic sediment layer appears in both holes as a carbonate spike at about 52 rmcd and provided an important tie point between the two holes. Note that the revised offsets in Table 9 are significantly different than the shipboard composite splice, especially from Core 167-1019C-4H and below.

We have good AMS radiocarbon age control from about 6 to 24 ka (2.9–12.1 rmcd; Mix et al., 1999) from 10 mixed planktic foraminifer samples, 10 mixed benthic foraminifer samples, and 1 piece of bark. We used these ages to constrain the Site 1019 age model for this time period. The radiocarbon dates indicate that early deglacial sedimentation rates rose to greater than 65 cm/k.y. The 5-cm depth resolution of our samples through this time period converts to a time resolution of 75 yr.

From the middle of MIS 3 to MIS 5d (~16–27 rmcd) sedimentation rates were significantly slower, as low as 14 cm/k.y. The typical 30-cm sample spacing in this depth interval spans ~2 k.y., and part of the problem we experience in correlating may occur because we have aliased peaks. We expected some slowdown in sedimentation in this interval because the 3.5-kHz seismic record of the upper sediments taken on the approach to Site 1019 shows a pinchout in the interval between ~20 and 32 mbsf (~ 20–34 rmcd; Fig. 8) with the strongest pinchout between ~21 and 27 mbsf (~21.3–28.5 rmcd). We have constructed a preliminary age model (Table 9), but expect that the 50- to 250-ka interval will be adjusted as more high-resolution data becomes available.

Site 1011

Because the sedimentation rate at Site 1011 is slow when compared to the northern sites (average of 4.3 cm/k.y. over the last 340 k.y., Table 10) and because there is a likelihood that the carbon records could change as we move south, the primary correlation tool we used is the benthic oxygen isotope record. Once we established a preliminary age model in this manner we adjusted the records to a minor extent to match $CaCO_3$ and C_{org} peaks.

Y74-2-22PC

Y74-2-22PC, near the tip of the Baja California Peninsula (Fig. 1) is our southernmost core and the core with the slowest sedimentation rate, averaging 1.3 cm/k.y. over the last 660 k.y. (Table 11). Although this core is unsuitable for k.y.-scale comparisons, it does allow us to monitor general trends. We also used the benthic oxygen isotope record at this core as the primary correlation tool to construct an age model and made minor adjustments to match carbon peaks.

MASS ACCUMULATION RATES

We have constructed mass accumulation rates (MARs) for the cores for the 0–140 ka period for which we have confidence in our age model. In each case the MAR is calculated from the product of the sedimentation rate, the percentage, and the dry bulk density (grams of sediment per cubic centimeter of original wet sample). For all sites except Cores W8709-13 and Y74-2-22 we estimated the dry bulk density from GRAPE wet bulk density because we had measure-

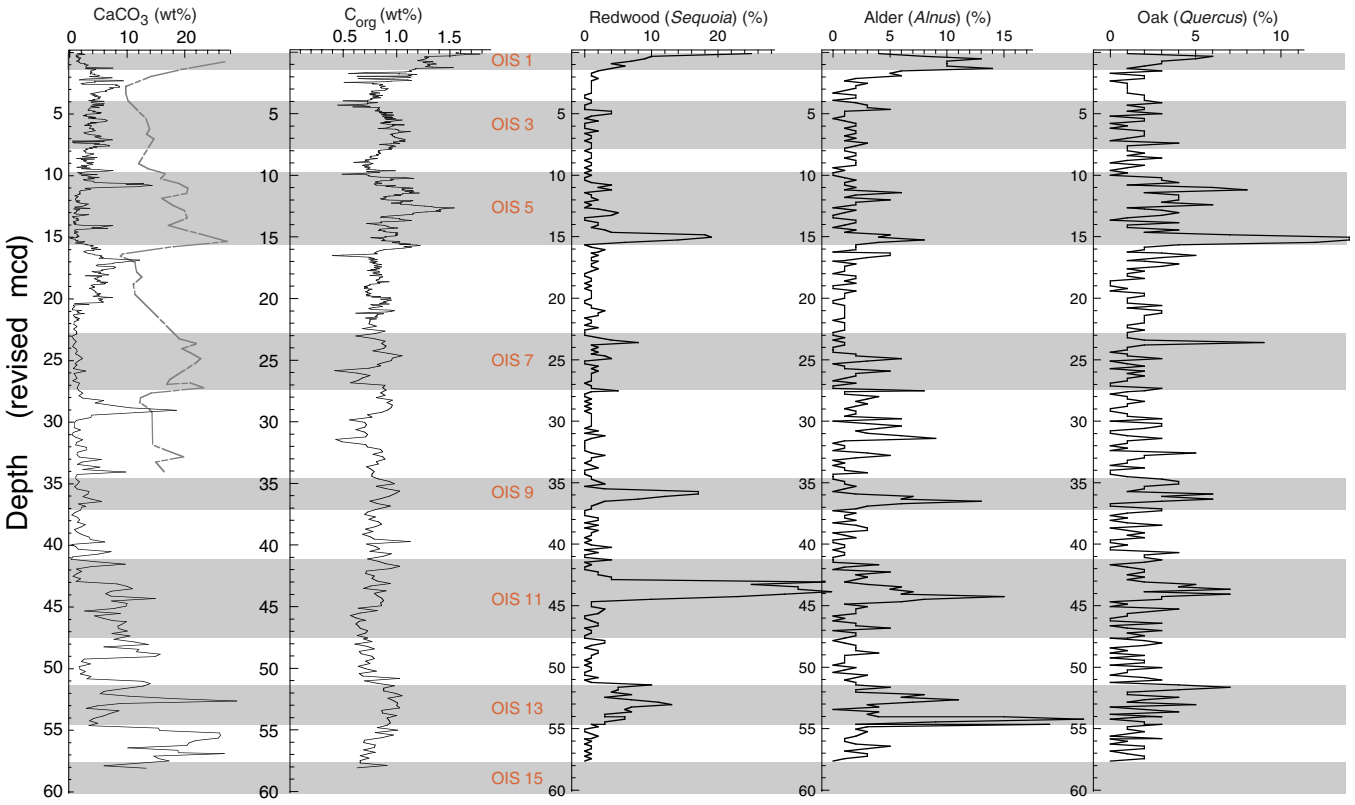

Figure 7. Pollen records from Site 1020 shown with carbon time series; preliminary oxygen isotope control is shown as the gray line with $CaCO_3$. The pollen records were used to mark strong interglacials and develop a preliminary time scale below oxygen isotope control.

ments at essentially all of our sample depths from MST analyses. The estimate is based on a linear correlation between wet and dry bulk density:

$$\rho_{dry} = 1.563\ \rho_{wet} - 1.560. \quad (1)$$

For both Cores W8709-13 and Y74-2-22, we estimated a change of dry bulk density with depth by comparison to nearby cores or drill sites where physical properties data were available.

We constructed MARs because MAR time series are independent of the behavior of other sedimentary components, provided that the age model is accurate. $CaCO_3$ and C_{org} weight percent time series may be driven by changes in dilution by other components, especially in slope sediments dominated by terrigenous clays and other aluminosilicates. Figure 9 shows the record at Site 1019, which was most strongly affected by changes in terrigenous sedimentation. The $CaCO_3$ MAR peak near the last glacial maximum all but disappears in the weight percent time series because of the huge increase in terrigenous sediment burial during this interval.

Fortunately, most of the cores had less extreme changes in sedimentation rates than Site 1019, and most records resembled those of Site 1020 (Fig. 10). The conversion to MAR makes little difference in the variance in the $CaCO_3$ time series, because the $CaCO_3$ weight percent peaks are a factor of 2–5 higher than the surrounding intervals, whereas the sedimentation rate varies by only about a factor of 2. The sedimentation rate model also has its dominant variance at lower frequencies than the carbonate events. The MAR conversion is more important for C_{org}, because the change in C_{org} weight percent is of the same magnitude as the change in sedimentation rates, and the dominant frequencies for variation are more similar in both time series.

The net effect of conversion to MAR is that all the carbon time series develop a stronger coherence to each other. Part of the increased

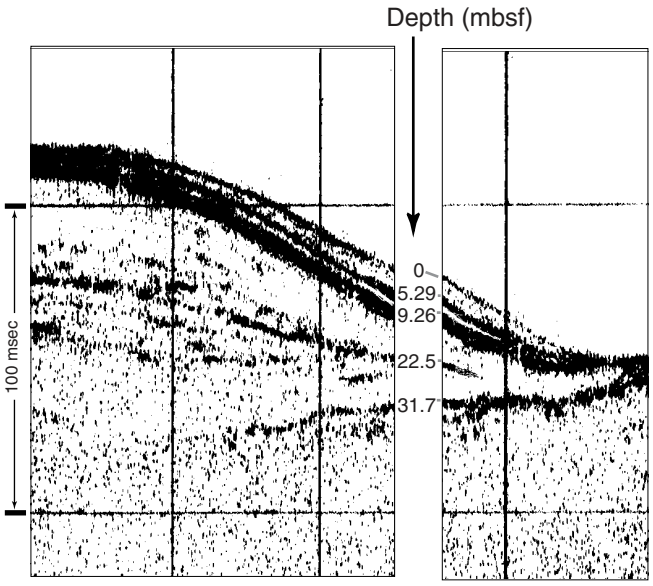

Figure 8. 3.5-kHz sub-bottom profile from *JOIDES Resolution* as it crossed Site 1019, showing the pinchout in sediments from roughly 20 to 30 mbsf. We assumed in our age model that this interval had reduced sedimentation rates compared to other intervals. Depths in the figure were calculated assuming a seismic velocity of 1560 m/s in the sediments.

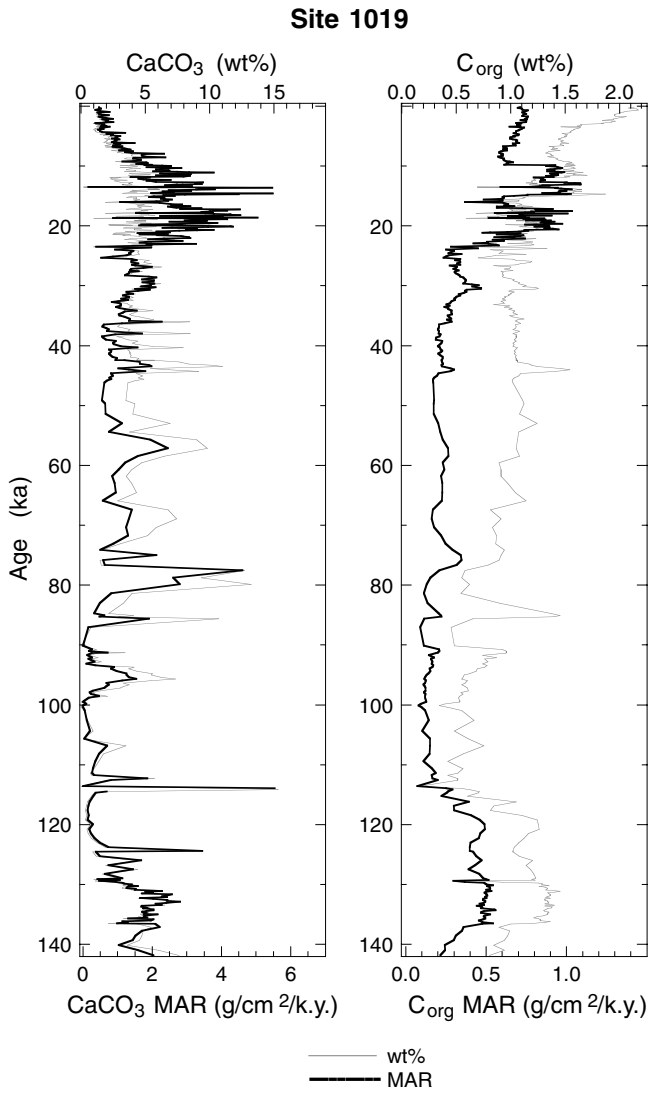

Figure 9. $CaCO_3$ and C_{org} time series for Site 1019, shown as weight percent and as mass accumulation rate (MAR). This site had major variations in sedimentation rate caused by highly variable sedimentation of terrigenous aluminosilicates. The sedimentation rate changes masked the flux variations of $CaCO_3$ and C_{org}.

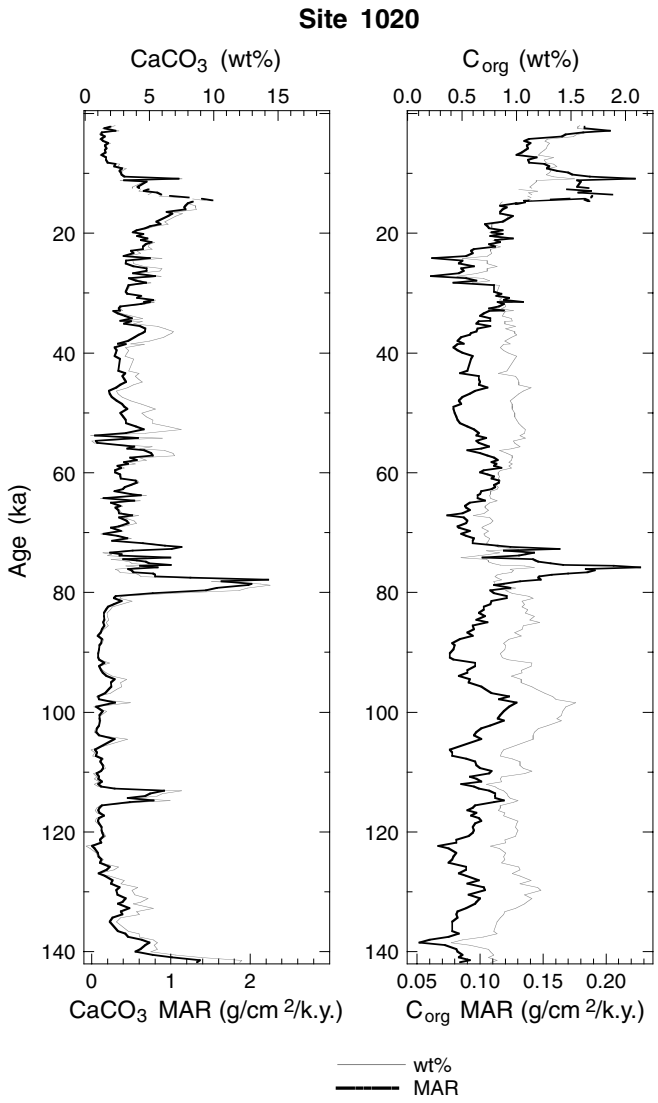

Figure 10. $CaCO_3$ and C_{org} time series for Site 1020, shown as weight percent and as mass accumulation rate (MAR). This site is more typical of the Leg 167 sites. Sedimentation rates varied by about a factor of two. Because of the large changes in $CaCO_3$ weight percent the MAR and weight percent time series have virtually the same variance, while the C_{org} MAR time series is significantly affected by both sedimentation rate and changes in weight percent.

coherence comes from use of a common age model, which, if wrong, will contaminate all the records with spurious peaks. However, more of the improvement comes from the removal of dilution artifacts in the weight percent record, as Figure 9 demonstrates.

STACKING THE 0–140 KA WEIGHT PERCENT AND MAR RECORDS

One of the purposes of this paper is to develop a high-resolution time series of k.y.-scale events. In the data sets we have collected, we have sufficient high-quality records for 0–140 ka, for which we have high confidence in our age model, to stack the records (four time series for $CaCO_3$; three for C_{org}) and substantially improve the signal to noise in our records. We will use this "Northern California Stack" to compare with events in the North Atlantic, like the Dansgaard/Oeschger events.

We have stacked both weight percent and MAR data, and we have designated names and ages for peaks in the percentage data based upon our age model (Tables 12, 13; Figs. 11, 12). We standardized the data before stacking by subtracting the mean of the time series from each data point and dividing by the standard deviation so that all time series are expressed in units of standard deviation from the mean. We interpolated each of the time series in the stack to an even 0.5-k.y. spacing, then summed each interval and divided by the number of records in that interval.

THE $CaCO_3$ RECORD COMPARED TO GREENLAND ICE CORES

Behl and Kennett (1996) have correlated oxygenation events in the Santa Barbara Basin to Dansgaard/Oeschger warming events found in Greenland ice cores. Lund and Mix (1998) in contrast reported that carbon isotope heavy excursions in the deep-water Core W8709-13 matched stadial episodes in North Atlantic records. The

Northern California stacks shown in Figure 11 exhibit events that are reminiscent of North Atlantic instability and can be directly compared in Figure 13.

Within the interval between 75 and 10 ka we observe a similarity between high $CaCO_3$ events and Dansgaard/Oeschger interstadials as recorded in the GISP-2 ice core (k.y.-scale warming events in Greenland; Grootes et al., 1993; Stuiver et al., 1995; time scales of Meese et al., 1994, and Sowers et al., 1993), although there are significant differences between the two records. We have not adjusted the records to improve the match, except perhaps indirectly through the use of Core W8709-13 as the primary age model in most of this period (Lund and Mix, 1998).

Table 12. Designation of C_{org} and $CaCO_3$ peaks in the stack record and age assignations from the age model developed in this paper.

C_{org} peak designation	$CaCO_3$ peak designation	Age of peak (ka)
OC 1-1		2.8
OC 1-2a		8.7
	CC 1-1	9.2
OC 1-2b		10.8
OC 1-2c		13.1
	CC 2-1	16.6
OC 2-1		21.6
	CC 2-2a	21.8
	CC 2-2b	23.4
OC 3-1		25.4
	CC 3-1	25.8
OC 3-2		31.4
	CC 3-2	31.4
	CC 3-3	36.5
OC 3-3		36.9
OC 3-4		42.5
	CC 3-4	44.3
OC 3-5		46.3
	CC 3-5a	49.3
	CC 3-5b	52.6
OC 3-6		53.8
	CC 3-5c	56.9
OC 3-7		58.1
	CC 4-1	60.9
OC 4-1		61.4
	CC 4-2	65.2
OC 4-2		67.2
	CC 4-3	68.0
	CC 4-4	72.3
OC 4-3		73.0
	CC 5-1	75.1
OC 5-1		75.7
	CC 5-2	78.9
OC 5-2		80.7
OC 5-3		84.9
OC 5-4		92.3
	CC 5-3	94.8
OC 5-5		99.0
	CC 5-4	104.6
OC 5-6		109.7
	CC 5-5	113.5
OC 5-7		119.0
	CC 5-6	124.3
OC 5-8		129.4
	CC 6-1	132.9

Notes: OC = organic carbon, CC = calcite. First number is oxygen isotope stage where peak lies, second number is numerical order in that isotope stage.

The most obvious differences in the records are the amplitudes of events around the carbonate peak CC 3-3 (30–45 ka) and on both the MIS 5/4 glaciation and on the MIS 2/1 deglaciation. The largest $CaCO_3$ peak in the MIS 5/4 glaciation interval, CC 5-2, has no counterpart in the Greenland oxygen isotope record, but a series of events from CC 5-1 (75.1 ka) through CC 3-5 (49 ka) mimic the Dansgaard/Oeschger interstadials. Events in the ice-core record may appear in the northern California $CaCO_3$ stack in the late MIS 3 and MIS 2 interval, but the amplitudes are clearly much lower. The early deglaciation around $CaCO_3$ peak CC 2-1 (18–12 ka) is made up of at least two oxygen isotope events in GISP-2 rather than the one large event we observe, but the younger Dryas (~13 ka) can be detected in both records. Before 85 ka there is little similarity between the two records, perhaps because only near-glacial conditions trigger a coherent response in both time series.

Clearly, the two records have some forcing in common but other factors limit the coherence between the time series. Determining these factors must in part depend upon determining the processes that produce the carbonate record. As always, the question arises whether the $CaCO_3$ record is produced by production or dissolution. Production implies a surface ocean link and a possible atmospheric connection to the North Atlantic. Dissolution, in contrast, implies a deep ocean connection perhaps linked to fluctuations in production of North Atlantic Deep Water.

The comparison between the $CaCO_3$ and C_{org} MAR time series (Fig. 14) shows no strong relationship between them, as would be expected if $CaCO_3$ burial were driven by a simple link to productivity. C_{org} percentages are generally higher in interglacials but the MAR does not show a clear trend, indicating that the percentage data is affected by dilution with terrigenous detritus. In contrast, both $CaCO_3$ MAR and percent are typically higher in glacials.

Strong $CaCO_3$ MAR events occur sometimes when there is moderately high C_{org} MAR (e.g., CC 3-3 at 36.5 ka). At other times $CaCO_3$ and C_{org} MAR events alternate in strength (e.g., MIS 5/4 boundary, 70–85 ka; MIS 2/1 interval, 25–8 ka). Despite the lack of a simple link between $CaCO_3$ burial and productivity, we have other evidence that has convinced us that the k.y.-scale events are driven by production, not dissolution.

PRODUCTION VS. DISSOLUTION IN THE DEVELOPMENT OF THE $CaCO_3$ TIME SERIES

We have three basic lines of evidence to show that $CaCO_3$ production and, probably, an increase in $CaCO_3$ production relative to total productivity is responsible for the $CaCO_3$ k.y.-scale events.

1. There is no depth response for at least the major $CaCO_3$ events.
2. If the Pleistocene $CaCO_3$ rain rate remained the same as modern rain rates, there is not enough $CaCO_3$ produced to make the events even with $CaCO_3$ saturation of the deep waters.
3. The modern distribution of $CaCO_3$ production with latitude and distance from shore can be used to make a reasonable hy-

Table 13. Carbon stacks, expressed as standardized scores.

Interpolated age (ka)	C_{org} % stack standardized	Number of records	$CaCO_3$ % stack standardized	Number of records	C_{org} MAR stack standardized	Number of records	$CaCO_3$ MAR stack standardized	Number of records
0.00	2.82	1	–1.34	1	–0.08	1	–1.10	1
0.50	2.67	1	–0.95	1	0.01	1	–0.90	1
1.00	3.05	1	–0.99	1	0.25	1	–0.91	1
1.50	3.29	1	–1.01	1	0.35	1	–0.92	1
2.00	3.32	2	–0.85	2	1.49	2	–0.80	2
2.50	3.33	2	–1.05	2	1.42	2	–0.92	2
3.00	3.57	2	–0.89	2	1.56	2	–0.81	2
3.50	2.83	2	–1.06	2	1.09	2	–0.95	2
4.00	2.18	2	–1.07	2	0.81	2	–0.94	2
4.50	1.55	2	–1.06	2	0.46	2	–0.94	2

This is a sample of the table that appears on the volume CD-ROM.

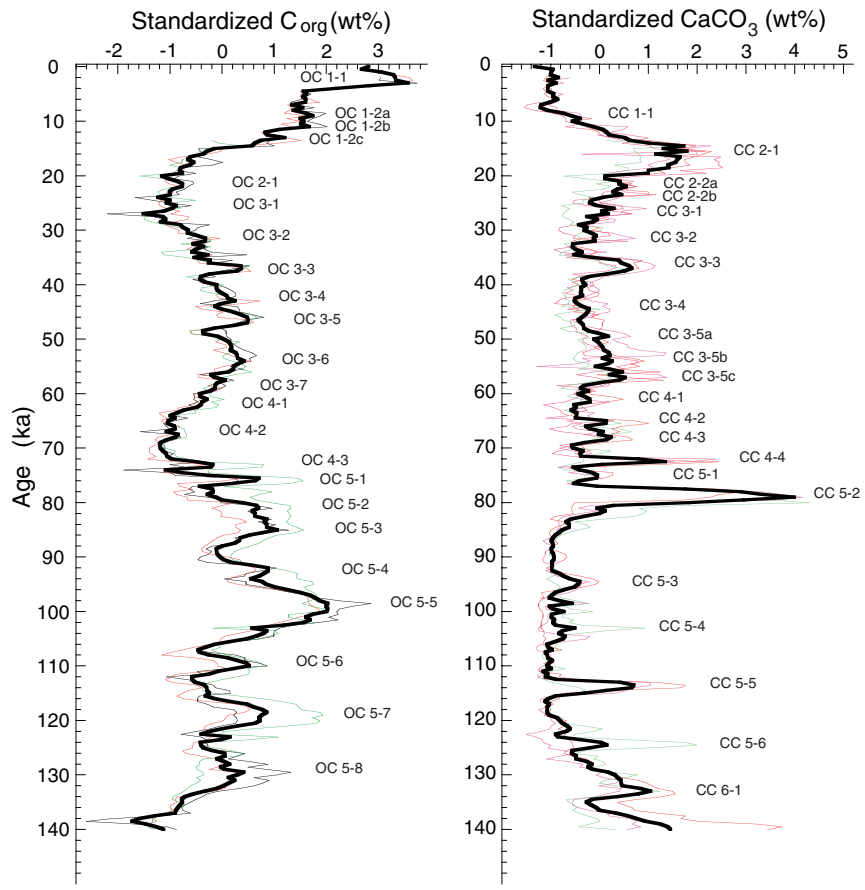

Figure 11. Stack of three C_{org} weight percent time series (Core EW9504-17, Site 1020, and Site 1018) and four $CaCO_3$ weight percent time series (the three above and Core W8709-13). Bold line = the stacked data; light lines are individual core or site records. Units are standard deviations from the mean of the time series. Named peaks are chronostratigraphic and can be used to correlate between sites.

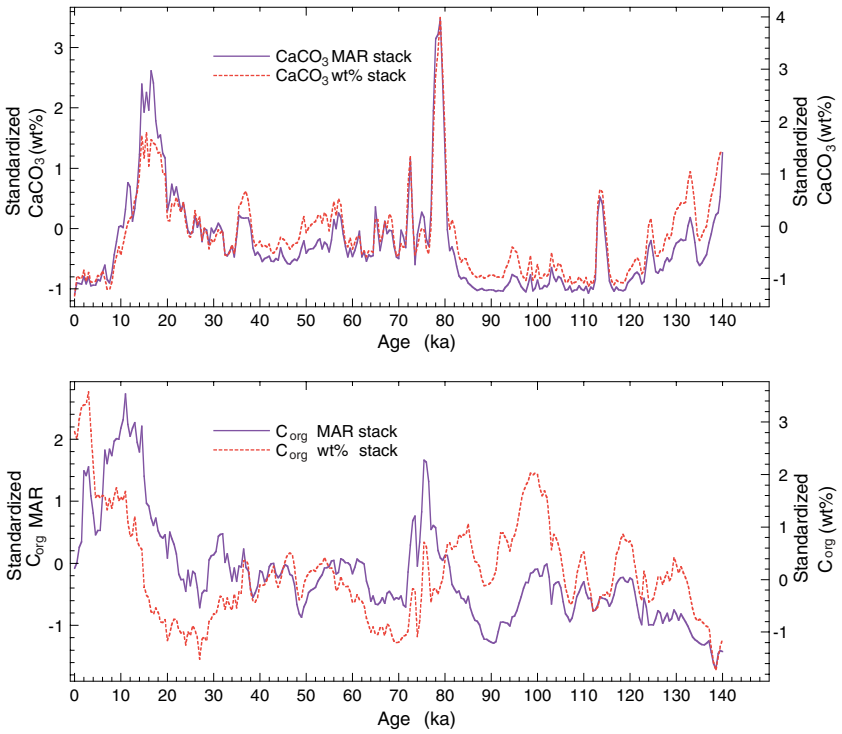

Figure 12. Comparison of weight percent and MAR stacks. The $CaCO_3$ weight percent and MAR stacks are virtually identical, whereas the sedimentation rate has a stronger influence upon the C_{org} MAR stack.

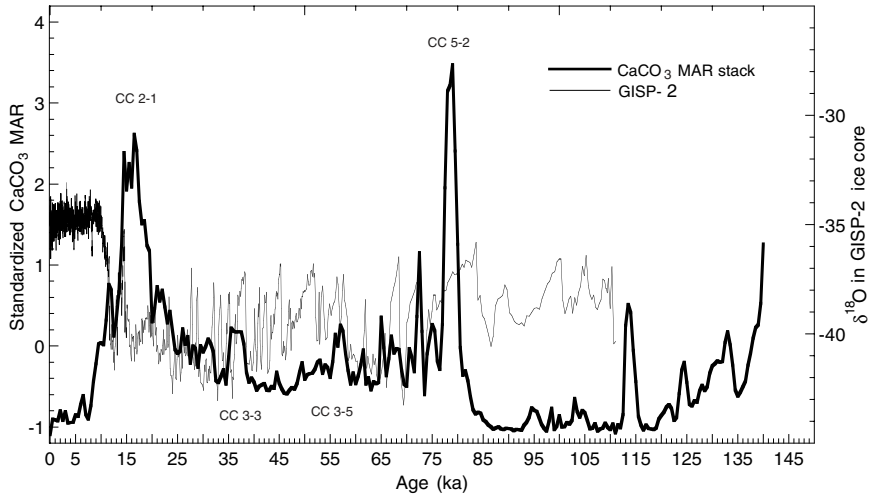

Figure 13. Comparison between the Northern California $CaCO_3$ stack (bold line) and GISP-2 Greenland ice-cap oxygen isotope record. Timing of events is similar in the period between 20 and 75 ka, although amplitudes may differ significantly.

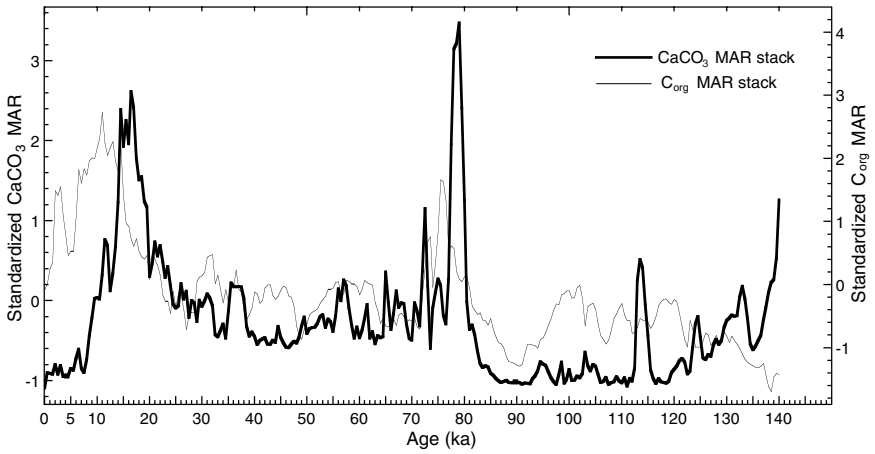

Figure 14. Comparison of Northern California $CaCO_3$ and C_{org} MAR stacks to show that the two time series have no simple relationship to each other. $CaCO_3$ MAR events tend to lead C_{org} MAR events by ~ 2 k.y.

pothesis for increased $CaCO_3$ production and burial during the k.y.-scale events.

Carbonate Burial at the Seafloor

There is a large body of literature on the geochemical processes that control dissolution, and we will not review it here. $CaCO_3$ burial is basically a competition between the processes that bring $CaCO_3$ to the seafloor and those that destroy it at the bottom. A simple-minded mass balance can be stated as follows:

$$CC_{burial} = CC_{rain} - f(C_{org\ rain}) - CC_{inorganic}, \quad (2)$$

where CC stands for $CaCO_3$ flux, rain refers to the fall of particulate matter to the bottom from the surface ocean, $f(C_{org\ rain})$ is the function that describes dissolution of $CaCO_3$ within sediments by organic matter degradation, and $CC_{inorganic}$ refers to the dissolution flux by inorganic processes related to changes in calcite saturation of deep ocean waters. Archer (1991b) estimates that 30%–50% of the total $CaCO_3$ that reaches the seafloor dissolves because of oxic degradation of organic matter, so it is clear that productivity can have both a positive effect (higher $CaCO_3$ rain to the bottom) and a negative one (higher $CaCO_3$ dissolution because of C_{org} degradation). To achieve a high burial rate of $CaCO_3$, high productivity is needed but with a high C_{CO_3}/C_{org} in the particulate rain from the euphotic zone.

The California margin is highly susceptible to $CaCO_3$ dissolution by C_{org} degradation, because it is a region of high C_{org} rain relative to $CaCO_3$ (C_{CO_3}/C_{org} is ~0.5, Dymond and Lyle, 1994) as compared to the tropical Pacific (C_{CO_3}/C_{org} is ~2.0). A change in $CaCO_3$ burial in the California margin could either reflect a change in rain of $CaCO_3$ relative to C_{org} or, conversely, small-scale temporal changes in inorganic dissolution.

The geochemical processes controlling inorganic dissolution in the oceans and their glacial-interglacial changes have been relatively well investigated. However, almost nothing is known about the processes that cause high $CaCO_3$ production relative to C_{org}, and how those processes might change through time. The basic implication of a change in $CaCO_3$ production without an equivalent change in C_{org} production is that there must be a reorganization of the plankton ecosystem with a shift towards conditions that favor coccolithophorids and foraminifers in contrast to primary producers and zooplankton that do not produce carbonate, such as diatoms, radiolarians, or other "bare" algae.

Northern California Depth Transect

The first line of evidence we present for a production control of the $CaCO_3$ time series is a depth transect near Cape Mendocino (Fig. 15: Site 1019, 988 m; Site 1018, 2476 m; Site 1020, 3038 m; and Site 1021, 4212 m). We observe no trend with depth in terms of $CaCO_3$ MAR for the k.y.-scale events, even though depth-dependent dissolution shapes the overall record of the deeper drill sites. Site 1021, the deepest of the northern California drill sites, best illustrates the depth effect. It has a much lower average $CaCO_3$ MAR than any of the other sites in the depth transect and is very near the local carbonate compensation depth (Karlin et al., 1992).

When the k.y.-scale events are examined, we find that $CaCO_3$ MAR peaks for which we have highest confidence (e.g., CC 2-1,~16

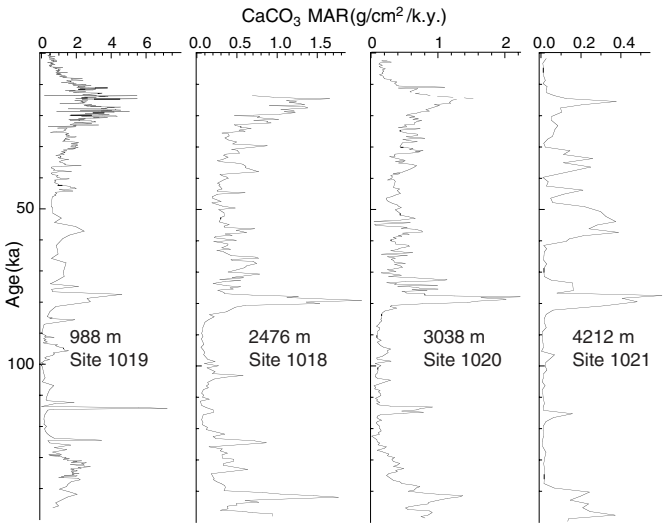

Figure 15. Depth profile of $CaCO_3$ MAR from cores from the northern and central California margin. Major peaks can be found at all depths, suggesting that the origin of the peaks is from the surface.

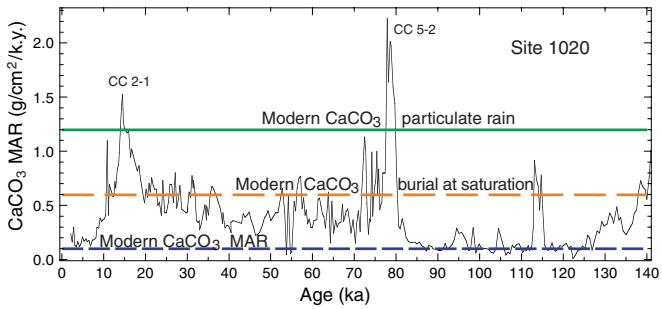

Figure 16. Comparison of k.y.-scale $CaCO_3$ MAR events at Site 1020 to $CaCO_3$ rain measured by sediment traps and to our calculations of $CaCO_3$ burial at calcite saturation (see text). Carbonate events CC 2-1 and CC 5-2 are larger than the modern $CaCO_3$ rain and must have been caused by changes in $CaCO_3$ production. A majority of the other k.y.-scale events are larger than the $CaCO_3$ MAR when deep ocean waters are saturated with respect to $CaCO_3$ and are most probably caused by changes in $CaCO_3$ production.

ka, with radiocarbon age control) is a factor of three higher than the average MIS 2 or early MIS 3 $CaCO_3$ MAR no matter what water depth the drill site is located in. There is no obvious change in preservation with depth, as would be expected if the $CaCO_3$ MAR were controlled by inorganic dissolution.

The major flaw with this argument is that the depth of calcite saturation in the North Pacific is relatively shallow, on the order of 700–800 m near the California margin based upon $[CO_3]^=$ data presented in Feely et al. (1984) and a $[CO_3]^=_{sat}$ for calcite at ~1000 m (100 bar pressure) and 5°C of 63 mmol/kg, calculated from equations in Pytkowicz (1969). All sites in the depth transect are beneath ocean waters undersaturated with respect to calcite, although Site 1019 should be minimally affected.

How Much Can Inorganic Dissolution Affect the Time Series?

The second line of evidence for production control of the $CaCO_3$ MAR time series is based upon a combination of sediment trap data near Site 1020 (Lyle et al., 1992; Dymond and Lyle, 1994) and chemical arguments. We show that many of the peaks in the Site 1020 $CaCO_3$ MAR record are larger than can be supported by changes in dissolution alone acting upon the modern $CaCO_3$ particulate rain to the seafloor.

Archer (1991a) summarized arguments of change in deep-water $[CO_3]^=$ on glacial-interglacial time scales and came to the conclusion that glacial Pacific deep water was enriched in $[CO_3]^=$ by about 7–11 µmol/kg. At the depth of Site 1020, $[CO_3]^=$ is about 8 µmol/kg less than calcite saturation (43 vs. 51 µmol/kg at saturation; calculated from data in Pytkowicz, 1969). The glacial/interglacial changes in ocean chemistry should have driven the 3-km horizon of the North Pacific essentially to saturation with calcite. If inorganic dissolution rather than production is the primary control of the $CaCO_3$ record, one should have a record marked by events reaching saturation, or roughly reaching the same $CaCO_3$ MAR.

We can also calculate the approximate size of a saturation $CaCO_3$ MAR event based upon nearby sediment trap data and rough estimates of the effect of C_{org} degradation on $CaCO_3$ preservation (Fig. 16). Two multiyear sediment-trap deployments were taken as part of the Multitracers project about 100 km north of Site 1020 (Lyle et al., 1992; Dymond and Lyle, 1994). The average $CaCO_3$ rain (Dymond and Lyle, 1994) was 1.5 g/ cm²/k.y. at the Nearshore site (125°45´ W) and 0.9 g/cm²/k.y. at the Midway site (127°35´ W). Site 1020 should have a $CaCO_3$ rain rate that is the average of these two, because it is in between them, or about 1.2 g/cm²/k.y. Of this fraction, essentially none (only about 0.1 g/cm²/k.y.) gets buried in the sediments today. Approximately 1.1 g/cm²/k.y. of the $CaCO_3$ rain dissolves at the seafloor, but only a fraction of this is dissolved by inorganic processes. Archer (1991b) estimated that 30%–50% of the total $CaCO_3$ rain falling to the seafloor is dissolved by CO_2 released by the oxic degradation of C_{org} rain, the magnitude depending upon the C_{CO_3}/C_{org} ratio. The ratio we have observed at both Nearshore and Midway is larger than Archer modeled, so we expect that the dissolution by C_{org} rain is roughly half of the total $CaCO_3$ rain. This leaves only about 0.5 g/cm²/k.y. to be dissolved by inorganic processes. By this back of the envelope calculation, all $CaCO_3$ MAR peaks >0.6 g/cm²/k.y. are too large to have been caused by changes in calcite saturation alone.

The "saturation" $CaCO_3$ MAR of 0.6 g/cm²/k.y. is near the baseline $CaCO_3$ MAR at Site 1020 for MIS 2, 3, and 4 (Fig. 16) in accord with a scenario where glacial Pacific deep water neared calcite saturation. Most of the $CaCO_3$ MAR peaks in the last 140 k.y., however, are larger than expected if $CaCO_3$ MAR were responding to saturation of deep water alone. Two peaks in particular, CC 2-1 and CC 5-2, are significantly larger than the modern $CaCO_3$ particulate rain. They can only have been caused by a combination of increased $CaCO_3$ production and reductions of both inorganic and organically mediated dissolution. Other peaks above the saturation line must have been driven either by changes in the magnitude of $CaCO_3$ particulate rain or by strong relative reductions of C_{org} particulate rain to reduce the organically mediated dissolution in the sediments.

The k.y.-scale $CaCO_3$ MAR events were probably caused by a change in plankton community and a resultant increase in $CaCO_3$ production and/or increase in C_{CO_3}/C_{org} in the particulate rain rather than because of an overall increase in primary productivity. There is definite structure to the MAR profiles that suggest an evolution of the surface conditions rather than diagenesis within the sediments. The $CaCO_3$ MAR peaks typically do not coincide with C_{org} MAR peaks although there is a relationship between the two. A cross spectral analysis of the stacked C_{org} and $CaCO_3$ MAR time series indicates that typical Milankovitch periods have significant coherence (Fig. 14), and periods at ~11, ~5, ~4, and ~ 1.6 k.y. However, the $CaCO_3$ MAR record leads the C_{org} MAR record by about 2 k.y. at all significant periods except the 1.6 k.y. period. Clearly, k.y.-scale $CaCO_3$ events are not high C_{org} events.

Ortiz et al.(1997) have already proposed a mechanism for higher $CaCO_3$ production relative to C_{org} in the glacial northeastern Pacific based upon shifts from coastal upwelling to more diffuse curl-of-windstress upwelling offshore. Ravelo et al. (1997) have also sug-

gested that anomalous late Pliocene $CaCO_3$ MAR may result from a similar change in ecosystem dynamics. We will amplify upon this hypothesis based upon our examination of modern sediment trap data.

Modern Distribution of $CaCO_3$ and C_{org} Geochemical Rain

It is possible to treat the k.y.-scale changes in surface oceanographic conditions to be equivalent to movements of modern north Pacific plankton communities over the positions of the Leg 167 drill sites. If this is so, one would expect that the Ortiz et al. (1997) model of increased curl-of-windstress upwelling at the last glacial maximum to be represented by an increase in the equivalent modern community now found offshore at the drill sites being studied. One would also predict that the modern offshore community should produce more $CaCO_3$ relative to C_{org}.

Subarctic radiolarian fauna were also an important part of the glacial plankton community, suggesting significantly colder water temperatures and subarctic oceanographic conditions (Moore, 1973; Prahl et al., 1995) so $CaCO_3$ and C_{org} production in the modern subarctic Pacific may be a useful indicator of production under glacial conditions along the northern California margin. One of the surprises of the modern sediment trap data set is the relative strength of $CaCO_3$ production in the northern Pacific.

A series of sediment trap experiments in the northeastern Pacific (Table 14; Martin and Knauer, 1983; Roth and Dymond, 1989; Lyle et al., 1992; Dymond and Lyle, 1994; Honjo et al., 1995) can be used to assess the modern $CaCO_3$ and C_{org} production. We have collated data from deep sediment traps in Table 14, to examine only the particulate rain and to avoid flux changes associated with the dynamics of the euphotic zone. Note that we list the mass flux of C associated with $CaCO_3$ in the table, not the $CaCO_3$ flux, for better comparison to the C_{org} flux. To obtain the $CaCO_3$ flux, multiply the C_{CO_3} flux by 8.33. Figure 17 shows the location of sediment traps on a map of the COADS February SST climatology and shows how the C_{CO_3}/C_{org} changes throughout the region. The February SST was chosen because this is usually reasonably close to the alkenone temperature recorded at the top of the nutricline where coccolithophorids are most abundant (Prahl et al., 1993; Doose et al., 1997).

C_{CO_3}/C_{org} is highest in the modern particulate rain away from the coastal upwelling region. The highest C_{CO_3}/C_{org} is in the north, with a peak around 48°N, not where waters are warmer. However, highest standing stocks of coccolithophorids in the north central Pacific are also found north of 45°N (Okada and Honjo, 1973), primarily consisting of the cosmopolitan species *Emiliana huxleyi*. Only one sediment trap experiment (NS) had higher $CaCO_3$ rain than the subarctic trap experiments JDF and PC85, and the NS mooring had a factor of 4 to 5 higher C_{org} rain than the subarctic traps. As far as $CaCO_3$ burial is concerned, a switch anywhere along the California margin to the offshore environment around 48°N would both increase absolute $CaCO_3$ rain and significantly reduce C_{org}-mediated losses from the sediments. It would be ideal to cause the k.y.-scale $CaCO_3$ events.

There is some slight evidence that peak $CaCO_3$ production relative to C_{org} may peak in the temperature range of 7°–9°C, the SST associated with the JDF and PC85 sediment trap moorings, because the ratio dips in the one sediment trap mooring to the north at 50°N (P82-84). This may be an artifact, however, because variability between years in this 3-yr P82-84 experiment was extremely high. In support of the idea that there is a moderate SST associated with peak $CaCO_3$ rain, we point out that we have noticed a correlation between the rate of C37 alkenone burial (a biomarker for coccolithophorids, Kreitz et al., Chap. 10, this volume) and $CaCO_3$ burial in preliminary data at Site 1020, with highest burial for both being associated with an alkenone-estimated SST between 8° and 10°C.

NORTH/SOUTH VARIATION OF TIME SERIES ALONG THE CALIFORNIA MARGIN

Now that we have established that the northern California $CaCO_3$ MAR time series are driven by changes in $CaCO_3$ production, what can we say about the coherence of these production events along the

Table 14. Northeastern Pacific sediment trap measurements of carbon rain.

Site	Latitude (°N)	Longitude (°W)	Trap depth (mbsl)	Distance from shore (km)	Deployment length (months)	C_{CO_3} rain rate (μg/cm²/yr)	C_{org} rain rate (μg/cm²/yr)	Source
Vertex I	35.7	123.8	>1700	35	~1	103	1113	Martin and Knauer, 1983
MFZ	39.5	127.7	3800	300	12	66	127	Dymond and Lyle, 1994
NS	42.1	125.8	2500	120	12	179	490	Dymond and Lyle, 1994
MW	42.2	127.6	2500	270	12	109	220	Dymond and Lyle, 1994
G	41.5	132.0	3400	660	12	50	90	Dymond and Lyle, 1994
JDF	48.0	128.1	2000	350	11	140	109	Dymond and Lyle, 1994
PC85	48.0	138.0	3500	750	12	148	120	Honjo et al., 1995
P82-84	50.0	145.0	3800	1250	36	80	127	Honjo et al., 1995

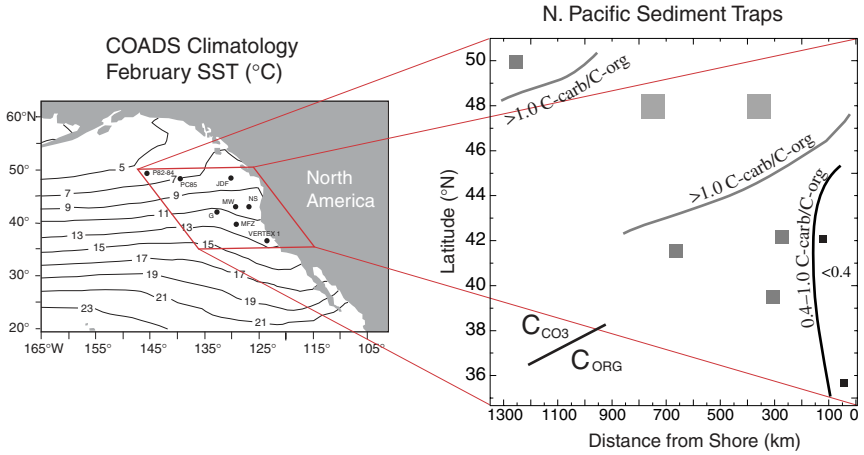

Figure 17. Modern sediment trap data from the northeastern Pacific showing how the ratio of $CaCO_3$ rain to C_{org} rain varies with distance from shore and latitude. High $CaCO_3$ rain occurs offshore out of the coastal upwelling region and in the northern part of the transition zone to the Alaska Gyre, where SST is between 7° and 9°C.

California margin? Unfortunately, we do not yet have any good high-resolution records from the south to compare with the drill sites >37°N. Figure 18 shows the two time series we now have from the south, at Site 1011 and at a piston core (Core Y74-2-22P) near the tip of Baja California. Both records have low resolution but show hints of at least some coherent response along the California margin.

The strong $CaCO_3$ event, CC 2-1 at 16.6 ka, is evident in all records and there is at least some $CaCO_3$ fluctuations near the MIS 4/5 boundary. Whether these represent $CaCO_3$ peaks like those seen in the north requires higher resolution time series than we have collected. Tentatively, we believe that echoes of the events in the north may be expressed in the southern California Current region, but the strength of the events appears to change along the margin.

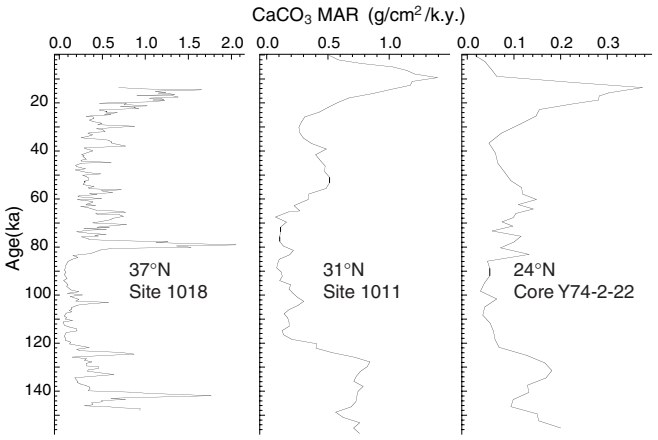

Figure 18. North-south transect of $CaCO_3$ MAR in cores along the California margin. The low resolution of the records we have in the south precludes k.y.-scale matchups. Nevertheless, some events prominent in the north appear to extend along the whole California Current.

DISCUSSION AND CONCLUSIONS

Our study has shown that k.y.-scale $CaCO_3$ and C_{org} events are a common feature of sediment records from the northern California margin for the late Pleistocene and that these events can be used with care for chronostratigraphic control. One should be aware that events do have different amplitudes at different drill sites. However, using both C_{org} and $CaCO_3$ for stratigraphic control alleviates most of the ambiguities.

We also conclude that the k.y.-scale $CaCO_3$ events are production driven, not caused by inorganic dissolution processes. The magnitude of the events are simply too large to be caused purely by changes in calcite saturation in North Pacific waters. We are less certain of the oceanographic processes that cause $CaCO_3$ events, but can hypothesize about changes in the structure of the North Pacific Ocean during typical glacial conditions as well as during the k.y.-scale events.

Surface Oceanographic Conditions Associated with k.y.-scale $CaCO_3$ Events

The $CaCO_3$ events are linked in some manner to the small interstadial Dansgaard/Oeschger events of the north Atlantic. Because the $CaCO_3$ events are driven by changes in production, there must have been significant changes on short time scales in the surface structure of the North Pacific. The lack of strong similarity between the $CaCO_3$ events and the Dansgaard/Oeschger events means that the climate of the North Pacific has been influenced by more than oscillations of the North Atlantic, however.

By comparison to the sediment trap studies we can at least present some hypotheses about surface oceanographic conditions along the California margin during average glacial conditions and during the k.y.-scale $CaCO_3$ events. High $CaCO_3$ burial implies that high C_{CO_3}/C_{org} conditions must have prevailed in the surface waters. In turn this must mean that coastal upwelling conditions along the California margin were severely weakened, as is also suggested by the lack of *Sequoia* in the glacial forests of northern California (Fig. 7; Sancetta et al., 1992). *Sequoia* require foggy conditions associated with cool summer upwelling for optimal growth.

The increase in C_{CO_3}/C_{org} implied by average glacial conditions as well as the k.y.-scale events could be explained in a scenario in which surface conditions block nutrients from reaching the uppermost euphotic zone, and in particular obligate nutrients favorable to the growth of large diatoms (Si, Dugdale, and Wilkerson, 1998; Berger and Lange, 1998; or Fe, Martin, and Fitzwater, 1988; Martin et al., 1991). Large diatoms are important exporters of organic matter from the euphotic zone. Removal of these species from the community significantly reduces the C_{org} rain and loss of nutrients from the euphotic zone while also increasing nutrient availability to other small phytoplankton like coccolithophorids. Increases in coccolithophorid community should increase the absolute flux of $CaCO_3$. The modern subarctic Pacific Ocean is dominated by small phytoplankton (Miller et al., 1991) and fits with this scenario.

Ortiz et al. (1997) suggested one means of limiting nutrients along the California margin, by slowing upwelling. Moving from a coastal upwelling regime to a curl-of-windstress upwelling regime will lower the net rate of upwelling and replacement of Si in the surface ocean. A second way to limit nutrients is to increase the stability of surface waters. Increasing the stability implies making the surface water fresher, because other evidence strongly favors significant glacial cooling of surface waters in the region of the northern California margin (Prahl et al., 1995; Doose et al., 1997; Kreitz et al., Chap. 10, this volume). Zahn et al. (1991) suggested that the glacial subarctic northeastern Pacific surface ocean was indeed fresher than the modern surface ocean and more stable, from oxygen isotope measurements upon planktic foraminifers. These waters, when advected into the northern California region and when the surface layer was warmed somewhat, would tend to be even more stable and conditioned for high $CaCO_3$ production.

A third way to limit critical nutrients is if the Fe flux to surface waters were reduced by limiting the aeolian atmospheric source or by weakening the local river source. The atmospheric source could be weakened either by moving the depocenter of Asian aeolian dust to the south of its present 40°N axis or by making the dust flux smaller. However, studies in the western Pacific indicate that the depocenter was stable in its latitudinal position and that glacial dust fluxes from Asia were significantly larger during glacials (Rea, 1994). The local riverine source of Fe was probably larger as well during glacials. Hovan et al. (Chap. 18, this volume) found that terrigenous deposition from a hemipelagic source was significantly higher at both Sites 1018 and 1020 during glacial periods.

Finally, one can decrease Si in upwelled waters by replacing the 100–200 m deep source water with a more Si-poor source (Berger and Lange, 1998). However, such a depletion should also affect the other nutrients, albeit to a lesser extent. One should observe both lower C_{org} rain and $CaCO_3$ rain in this scenario.

Based upon these observations, we believe that average glacial conditions could be governed by some combination of (1) an "offshore" scenario (Ortiz et al., 1997) in which the rate of ekman pumping of nutrients were diminished with (2) a "subarctic" scenario, in which a cold but relatively fresh surface layer existed. The k.y.-scale events were probably caused by slight improvements in conditions during minor northern hemisphere warmings—that is, injection of somewhat more nutrients into the euphotic zone but slightly less than the necessary level to allow diatoms to dominate. Although we cannot yet state with any certainty what these conditions would be, a slight average warming of the North Pacific should cause a net loss of fresh water to the North American ice cap and weaken the stability of the surface mixed layer somewhat. In addition, relatively small in-

creases in storm frequency or intensity could provide mixing events to support additional $CaCO_3$ production. Slight increases in northerly winds along the coast may have also contributed. These different hypotheses will be investigated in more detail during follow-up studies.

The change in plankton community would also explain why the $CaCO_3$ and C_{org} time series are significantly different, either because the C_{org} time series is a mixed signal of terrestrial and marine sources or because the production of $CaCO_3$ is not directly linked to primary productivity, but to the plankton community that is the producer. We argue against the strong influence of terrestrial C_{org}, because all of our time series have similar signals despite being located as much as 600 km apart.

ACKNOWLEDGMENTS

We gratefully acknowledge the help of our student analysts Ellen Unsworth, Debi Agenbroad, and Suzanne Shaub who ran the majority of the carbon analyses. This project was supported by JOI/USSP, and by NSF grants OCE-9634141 (Site Survey for Leg 167) and OCE-9811272 (millennial variations in California margin sediments). Samples from the piston cores were provided by the Oregon State University core laboratory (NSF Grant OCE-9712024).

REFERENCES

Archer, D., 1991a. Equatorial Pacific calcite preservation cycles: production or dissolution? *Paleoceanography,* 6:561–571.

————, 1991b. Modeling the calcite lysocline. *J. Geophys. Res.,* 96:17037–17050.

Behl, R.J., and Kennett, J.P., 1996. Brief interstadial events in the Santa Barbara Basin, NE Pacific, during the last 60 kyr. *Nature,* 376:243–246.

Berger, W.H., and Lange, C.B., 1998. Silica depletion in the thermocline of the glacial North Pacific: corollaries and implications. *Deep-Sea Res., Pt. II,* 45:1885–1904.

Doose, H., Prahl, F.G., and Lyle, M.W., 1997. Biomarker temperature estimates for modern and last glacial surface waters of the California Current system between 33° and 42°N. *Paleoceanography,* 12:615–622.

Dugdale, R.C., and Wilkerson, F.P., 1998. Silicate regulation of new production in the equatorial Pacific upwelling. *Nature,* 391:270–273.

Dymond, J., and Lyle, M., 1994. Particle fluxes in the ocean and implications for sources and preservation of ocean sediments. *In* Hay, W.W. (Ed.), *Material Fluxes on the Surface of the Earth:* Washington D.C. (National Academy of Science), 125–143.

Feely, R.A., Byrne, R.H., Betzer, P.R., Gendron, J.F., and Acker, J.G., 1984. Factors influencing the degree of saturation of the surface and intermediate waters of the north Pacific Ocean with respect to aragonite. *J. Geophys. Res.,* 89:10631–10640.

Gardner, J.V., Dean, W.E., and Dartnell, P., 1997. Biogenic sedimentation beneath the California Current system for the past 30 kyr and its paleoceanographic significance. *Paleoceanography,* 12:207–227.

Grootes, P.M., Stuvier, M., White, J.W.C., Johnsen, S., and Jouzel, J., 1993. Comparison of oxygen isotope records from the GISP2 and GRIP Greenland ice cores. *Nature,* 366:552–554.

Guyodo, Y., Richter, C., and Valet, J.-P., 1999. Paleointensity record from Pleistocene sediments (1.4–0 ma) off the California margin. *J. Geophys. Res.,* 104:22953–22964.

Honjo, S., Dymond, J., Collier, R., and Manganini, S.J., 1995. Export produciton of particles to the interior of the equatorial Pacific Ocean during the 1992 EqPac experiment. *Deep-Sea Res.,* 42:831–870.

Imbrie, J., Hays, J.D., Martinson, D.G., McIntyre, A., Mix, A.C., Morley, J.J., Pisias, N.G., Prell, W.L., and Shackleton, N.J., 1984. The orbital theory of Pleistocene climate: support from a revised chronology of the marine $\delta^{18}O$ record. *In* Berger, A., Imbrie, J., Hays, J., Kukla, G., and Saltzman, B. (Eds.), *Milankovitch and Climate* (Pt. 1), NATO ASI Ser. C, Math Phys. Sci., 126:269–305.

Karlin, R., Lyle, M., and Zahn, R., 1992. Carbonate variations in the Northeast Pacific during the late Quaternary. *Paleoceanography,* 7:43–61.

Kennett, J.P., Baldauf, J.G., and Lyle, M. (Eds.), 1995. *Proc. ODP, Sci. Results,* 146 (Pt. 2): College Station, TX (Ocean Drilling Program).

Lund, D.C., and Mix, A.C., 1998. Millennial-scale deep-water oscillations: reflections of the North Atlantic in the deep Pacific from 10 to 60 Ka. *Paleoceanography,* 13:10–19.

Lyle, M., Koizumi, I., Richter, C., et al., 1997. *Proc. ODP, Init. Repts.,* 167: College Station, TX (Ocean Drilling Program).

Lyle, M., Zahn, R., Prahl, F., Dymond, J., Collier, R., Pisias, N., and Suess, E., 1992. Paleoproductivity and carbon burial across the California Current: the Multitracers Transect, 42°N. *Paleoceanography,* 7:251–272.

Martin, J.H., and Fitzwater, S.E., 1988. Iron deficiency limits pytoplankton growth in the north-east Pacific subarctic. *Nature,* 308:621–624.

Martin, J.H., Fitzwater, S.E., and Gordon, R.M., 1991. We still say iron deficiency limits phy-toplankton growth in the subarctic Pacific. *J. Geophys. Res.,* 96:20699–20700.

Martin, J.H., and Knauer, G.A., 1983. VERTEX: manganese transport with $CaCO_3$. *Deep-Sea Res.,* 30: 411–425.

Martinson, D.G., Pisias, N.G., Hays, J.D., Imbrie, J., Moore, T.C., Jr., and Shackleton, N.J., 1987. Age dating and the orbital theory of the ice ages: development of a high-resolution 0 to 300,000-year chronostratigraphy. *Quat. Res.,* 27:1–29.

Meese, D., Alley, R., Gow, T., Grootes, P.M., Mayewski, P., Ram, M., Taylor, K., Waddington, E., and Zielinski, G., 1994. Preliminary depth-age scale of the GISP2 ice core. *CRREL.*

Miller, C.B., Frost, B.W., Booth, B., Wheeler, P.A., Landry, M.R., and Welschmeyer, N., 1991. Ecological processes in the subarctic Pacific: iron limitation cannot be the whole story. *Oceanography,* 4:71–79.

Mix, A.C., Lund, D.C., Pisias, N.G., Bodén, P., Bornmalm, L., Lyle, M., and Pike, J., 1999. Rapid climate oscillations in the northeast Pacific during the last deglaciation reflect northern and southern hemisphere sources. *In* Webb, R.S., Clark, P.U., and Keigwin, L. (Eds.), *Mechanisms of Millennial-scale Global Climate Change.* Geophys. Monogr., Am. Geophys. Union, 112:127–149.

Moore, T.C., Jr., 1973. Late Pleistocene-Holocene oceanographic changes in the northeastern Pacific. *Quat. Res.,* 3:99–109.

Okada, H., and Honjo, S., 1973. The distribution of oceanic coccolithophorids in the Pacific. *Deep-Sea Res. Part A,* 20:355–374.

Ortiz, J., Mix, A., Hostetler, S., and Kashgarian, M., 1997. The California Current of the last glacial maximum: reconstruction at 42 degree N based on planktonic foraminifera. *Paleoceanography,* 12:191–205.

Paillard, D., Labeyrie, L., and. Yiou, P., 1996. Macintosh program performs time-series analysis. *Eos,* 77:379.

Prahl, F.G., Collier, R.B., Dymond, J., Lyle, M., and Sparrow, M.A., 1993. A biomarker perspective on prymnesiophyte productivity in the northeast Pacific Ocean. *Deep-Sea Res. Part A,* 40:2061–2076.

Prahl, F.G., Pisias, N., Sparrow, M.A., and Sabin, A., 1995. Assessment of sea-surface temperature at 42° N in the California Current over the last 30,000 years. *Paleoceanography,* 10:763–773.

Pytkowicz, R.M., 1969. Chemical solution of calcium carbonate in sea water. *Am. Zool.,* 9:673–679.

Ravelo, A.C., Lyle, M., Koizumi, I., Caulet, J.P., Fornaciari, E., Hayashida, A., Heider, F., Hood., J., Hovan, S., Janecek, T., Janik, A., Stax, R., Yamamoto, M., and Leg 167 Scientific Party, 1997. Pliocene carbonate accumulation along the California margin. *Paleoceanography,* 12:729–741.

Rea, D.K., 1994. The paleoclimatic record provided by eolian deposition in the deep sea: the geologic history of wind. *Rev. Geophys.,* 32:159–195.

Roth, S.E., and Dymond, J., 1989. Transport and settling of organic material in a deep-sea hydrothermal plume: evidence from particle flux measurements. *Deep-Sea Res.,* 36:1237–1254.

Sancetta, C., Lyle, M., Heusser, L., Zahn, R., and Bradbury, J.P., 1992. Late-glacial to Holocene changes in winds, upwelling, and seasonal production of the Northern California current system. *Quat. Res.,* 38:359–370.

Sowers, T., Bender, M., Labeyrie, L., Martinson, D., Jouzel, J., Raynaud, D., Pichon, J.J., and Korotkevich, Y., 1993. 135,000 year Vostok-SPECMAP common temporal framework. *Paleoceanography,* 8:737–766.

Stuiver, M., Grootes, P.M., and Braziunas, T.F., 1995. The GISP2 Delta 18-O climate record of the past 16,500 years and the role of the sun, ocean, and volcanoes. *Quat. Res.,* 44:341–354.

Zahn, R., Pedersen, T.F., Bornhold, B.D., and Mix, A.C., 1991. Water mass conversion in the glacial subarctic Pacific (54°N, 148°W): physical constraints and the benthic-planktonic stable isotope record. *Paleoceanography,* 6:543–560.

Date of initial receipt: 15 October 1998
Date of acceptance: 10 May 1999
Ms 167SR-214